15 Siu MKY, Wong ESY, Chan HY *et al.* Differential expression and phosphorylation of Pak1 and Pak2 in ovarian cancer: effects on prognosis and cell invasion. *Int. J. Cancer* 2010; **31**: 21–31.
16 Siu MKY, Yeung MCW, Zhang H, Kong DSH, Chan DCW, Cheung ANY. p21-activated kinase-1 promotes aggressive phenotype, cell proliferation, and invasion in gestational trophoblastic disease. *Am. J. Pathol.* 2010; **176**: 3015–22.
17 Damdinsuren B, Nagano H, Kondo M *et al.* TGF-β1-induced cell growth arrest and partial differentiation is related to the suppression of Id1 in human hepatoma cells. *Oncol. Rep.* 2006; **15**: 401–8.
18 Zhan Q, Ge Q, Ohira T, Dyke TV, Badwey JA. p21-activated kinase 2 in neutrophils can be regulated by phosphorylation at multiple sites and by a variety of protein phosphatases. *J. Immunol.* 2003; **171**: 3785–93.
19 Wang S, Wilkes MC, Leof EB, Hirschberg R. Imatinib mesylate blocks a non-Smad TGF-β pathway and reduces renal fibrogenesis in vivo. *FASEB J.* 2005; **19**: 1–11.
20 Yan X, Zhang J, Sun Q *et al.* p21-Activated kinase 2 (PAK2) inhibits TGF-β signaling in Madin-Darby canine kidney (MDCK) epithelial cells by interfering with the receptor-Smad interaction. *J. Biol. Chem.* 2012; **287**: 13705–12.
21 Wilkes MC, Repellin CE, Hong M *et al.* Erbin and the NF2 tumor suppressor Merlin cooperatively regulate cell-type-specific activation of PAK2 by TGF-β. *Dev. Cell* 2009; **16**: 433–44.
22 Zaret KS. Hepatocyte differentiation: from the endoderm and beyond. *Curr. Opin. Genet. Dev.* 2001; **11**: 568–74.
23 Wu X-Z, Chen D. Origin of hepatocellular carcinoma: role of stem cells. *J. Gastroenterol. Hepatol.* 2006; **21**: 1093–8.
24 Hartsough MT, Mulderi KM. Transforming growth factor β activation of p44mapk in proliferating cultures of epithelial cells. *J. Biol. Chem.* 1995; **270**: 7117–24.
25 Chong C, Tan L, Lim L, Manser E. The mechanism of PAK activation. Autophosphorylation events in both regulatory and kinase domains control activity. *J. Biol. Chem.* 2001; **276**: 17347–53.
26 Bandapalli OR, Macher-Goeppinger S, Schirmacher P, Brand K. Paracrine signalling in colorectal liver metastases involving tumor cell-derived PDGF-C and hepatic stellate cell-derived PAK-2. *Clin. Exp. Metastasis* 2012; **29**: 409–17.
27 Ching YP, Leong VY, Lee MF, Xu HT, Jin DY, Ng IO. P21-activated protein kinase is overexpressed in hepatocellular carcinoma and enhances cancer metastasis involving c-Jun NH2-terminal kinase activation and paxillin phosphorylation. *Cancer Res.* 2007; **67**: 3601–8.
28 Coniglio SJ, Zavarella S, Symons MH. Pak1 and Pak2 mediate tumor cell invasion through distinct signaling mechanisms. *Mol. Cell. Biol.* 2008; **28**: 4162–72.
29 Siu MK, Wong ES, Chan HY *et al.* Differential expression and phosphorylation of Pak1 and Pak2 in ovarian cancer: effects on prognosis and cell invasion. *Int. J. Cancer* 2010; **127**: 21–31.

Supporting information

Additional Supporting Information may be found in the online version of this article at the publisher's web-site:

Figure S1 Western blot analysis of PAK2 siRNA-transfected HepG2 cells. After 24 h of transfection, cells were serum-deprived for 24 h and treated with TGF-β for 2 h. Columns show relative band intensities expressed as the fold changes relative to control cells. Data are expressed as mean ± SD of three independent experiments (NS, not significant).

Figure S2 Western blot analysis of PAK2 siRNA-transfected HepG2 cells. Twenty-four hours after transfection, cells were serum-deprived for 24 h before being treated with TGF-β for 2 h with or without a 1 h pretreatment with either LY294002 or NAC. Columns show relative band intensities expressed as the fold changes compared to control cells. Data are expressed as mean ± SD of three independent experiments ($^{**}P < 0.01$ vs non-treated cells: NS, not significant).

Figure S3 Cell migration assay of PAK2 siRNA-treated cells. Twenty-four hours after transfection, cells were treated with TGF-β for an additional 24 h with or without pretreatment with LY294002 or NAC for 1 h. The cells were suspended in DMEM containing 1% FBS and plated at 1×10^4 cells/mL in the upper chambers of transwell supports with 8-mm pores (BD Biosciences). The lower chambers were filled with medium containing 10% FBS. After 10 h, the cells that had migrated through the pores were counted in five random microscopic fields, and the average number of migrated cells in control siRNA-transfected wells was set at 100%. Data are expressed as mean ± SD of three independent experiments ($^{**}P < 0.01$ vs non-treated cells: NS, not significant).

Gene Therapy (2013), 1–8

www.nature.com/gt

ORIGINAL ARTICLE

Novel electric power-driven hydrodynamic injection system for gene delivery: safety and efficacy of human factor IX delivery in rats

T Yokoo[1,4], K Kamimura[1,4], T Suda[1], T Kanefuji[1], M Oda[2], G Zhang[3], D Liu[3] and Y Aoyagi[1]

The development of a safe and reproducible gene delivery system is an essential step toward the clinical application of the hydrodynamic gene delivery (HGD) method. For this purpose, we have developed a novel electric power-driven injection system called the HydroJector-EM, which can replicate various time–pressure curves preloaded into the computer program before injection. The assessment of the reproducibility and safety of gene delivery system *in vitro* and *in vivo* demonstrated the precise replication of intravascular time–pressure curves and the reproducibility of gene delivery efficiency. The highest level of luciferase expression (272 pg luciferase per mg of proteins) was achieved safely using the time–pressure curve, which reaches 30 mm Hg in 10 s among various curves tested. Using this curve, the sustained expression of a therapeutic level of human factor IX protein (>500 ng ml^{-1}) was maintained for 2 months after the HGD of the pBS-HCRHP-FIXIA plasmid. Other than a transient increase in liver enzymes that recovered in a few days, no adverse events were seen in rats. These results confirm the effectiveness of the HydroJector-EM for reproducible gene delivery and demonstrate that long-term therapeutic gene expression can be achieved by automatic computer-controlled hydrodynamic injection that can be performed by anyone.

Gene Therapy (2013) **0,** 000–000. doi:10.1038/gt.2013.2

Keywords: gene delivery; hydrodynamic gene delivery; hemophilia; human factor IX

INTRODUCTION

Gene therapy has shown promising results in treating major disease, including cancer, cardiovascular diseases and hemophilia,[1] and the popularity of gene therapy for these diseases continues to grow. Among the various methods of gene transfer, hydrodynamic gene delivery (HGD) was first reported to be a simple and effective gene delivery method for the mouse liver in 1999.[2,3] Since then, HGD has been extensively studied and used in small animals for various types of gene delivery research, including gene expression, gene functional analysis, gene regulation, drug metabolism, establishment of animal models, drug discovery, viral vectors and nanoparticles (for recent reviews, see Suda and Liu,[4] Herweijer and Wolff,[5] Kamimura and Liu,[6] Kamimura *et al.*[7] and Bonamassa *et al.*[8]). The method of HGD consists of the rapid and pressurized injection of a large amount of isotonic DNA solution into a target organ *via* vessels.[9–12] However, traditional HGD technology has not been directly applied to humans owing to safety issues related to an unexpected large volume and high intravascular pressure during gene delivery, and difficulty in maintaining reproducibility due to the variability of responsiveness to the pressure in target organs.

In the past decade, our team and others have improved several aspects of the HGD procedure in addressing these issues. First, a catheter-based procedure was included to reduce injection volume and achieve site-specific DNA delivery.[13–18] Eastman *et al.*[13] reported successful isolated liver-targeted HGD in rabbits with a volume of 15 ml kg^{-1}; Yoshino *et al.*[14] reported single-lobe-specific gene delivery in pigs using catheterization and occlusion of the portal vein (PV); and Alino *et al.*[15] reported successful gene delivery of the human α-1 antitrypsin gene by catheterization. Fabre *et al.*[16] isolated the liver by double occlusions in the inferior vena cava (IVC) and performed whole liver-targeted HGD from the IVC.[16] A recent report from Alino's group[19] demonstrated the efficacy of this procedure in *ex vivo* human liver segments.[19] Second, we developed a CO_2-pressurized injector, called the 'HydroJector', for a sustained injection power for the maintenance of injection parameters.[20] This injector cleared the problem of a sustained flow rate injection by traditional manual hydrodynamic injection or simple pump injection associated with high variability in gene expression *in vivo* due to resistance in the area.[14] We recently showed that these two improvements yield a catheter-based regional liver lobe-specific HGD by inserting the catheter into each hepatic vein followed by the CO_2-pressurized injection of gene delivery. We called this development the 'Image-guided regional HGD', and it achieved 100- to 1000-fold improved gene expression compared with previous reports,[14,15] with a volume of 1% body weight (BW) that was 10-fold less than was used in those reports. Moreover, the sequential injection of multiple lobes can be safely performed with this procedure.[17] We also reported the applicability of this procedure to swine muscle.[18] While carefully studying the physiological data and gene delivery efficiency of 'Image-guided regional HGD', we determined that the level of

[1]Division of Gastroenterology and Hepatology, Graduate School of Medical and Dental Sciences, Niigata University, Niigata, Niigata, Japan; [2]Institute for Research Collaboration and Promotion, Niigata University, Niigata, Niigata, Japan and [3]Department of Pharmaceutical and Biomedical Sciences, College of Pharmacy, University of Georgia, Athens, GA, USA. Correspondence: Dr K Kamimura, Division of Gastroenterology and Hepatology, Graduate School of Medical and Dental Sciences, Niigata University, 1-757 Asahimachi-dori, Chuo-ku, Niigata, Niigata 9518510, Japan.
E-mail: kenya-k@med.niigata-u.ac.jp
[4]These authors contributed equally to this work.
Received 9 October 2012; revised 21 November 2012; accepted 21 December 2012

gene expression in the liver lobe after HGD depends on the intravascular pressure upon injection, which is affected by various factors, including placement of the catheter, leakage to the IVC, intravenous anastomosis, balloon inflation and differences in histological structures such as fibrotic tissue.[17] For example, in swine liver, sustained injection power of 300 psi for 15 s resulted in luciferase activity of 10^7 relative light units (RLU) per mg of proteins in the right medial, left medial and left lateral lobes, and 10^4 level in the right lateral lobe. This 1000-fold difference was proven to be due to the anatomically larger number of leakage pathways to IVC of the solution from the right lateral lobe.[17] The time–pressure curve during these injections showed a sustained peak pressure of 75 mm Hg over the entire injection period in area achieved 10^7 level and an irregularly shaped curve reaching a peak pressure of 70 mm Hg in 5 s and declining slowly thereafter for 10 s was seen in 10^4 area. These results indicate that the time–pressure curve upon the injection is significantly related to gene delivery efficiency and reproducibility.[17,18]

Therefore, we realized that the remaining challenge for the use of the catheter-based 'Image-guided regional HGD' procedure in humans is to control the time–pressure curves for the precise reproducibility and controllability of gene delivery. For this purpose, we have developed a novel electric power-driven hydrodynamic injection system, called the HydroJector-EM, and evaluated its gene delivery efficiency, reproducibility and safety in this study. The significant advantage of this injector is its precise replication of time–pressure curves that have been preloaded into the program for various targets by flexibly controlling the injection power. This has never been achieved with a manual injection or a simple pump. Furthermore, the HydroJector-EM consists of clinically approved parts and disposable products, such as syringes and injection tubes, for future clinical applications. Here we report for the first time the precise reproducibility and controllability of safe and efficient HGD using our new system. Our long-term study demonstrated sustained therapeutic gene expression of human factor IX in rats. The results indicate that anyone can achieve safe, efficient and therapeutic HGD using this new system; thus, the clinical applications of HGD procedures can be realized.

RESULTS

A major obstacle in developing clinically applicable HGD technology is precise reproducibility of gene delivery and safety of the procedure. The HydroJector-EM developed in this study can precisely replicate time–pressure curves that have been preloaded into the program and reproduces safe and effective gene delivery.

Development of the new gene injector

A major advantage of the HydroJector-EM is the flexible and fine computer control of the injection power to replicate precisely the programmed time–pressure curves for safe, efficient and reproducible gene delivery, which is unable to be achieved by the manual or the simple pump. In this new system, firstly we preload time–pressure curves before injection (Figure 1a, Step 1). Then, the electric power-driven injector pushes a sterilized syringe and injects its solution into the target region (Figure 1a, Step 2). The actual pressure in the target region during injection is transmitted to the programmed computer every 0.05 s through a pressure sensor placed in the vasculature connected to the target organ, such as PV in the liver, and amplifier (Figure 1a, Step 3). The system employs a pulse-width modulation control according to the pressure, and a program stored in the computer moves the syringe set in the injector and produces a preloaded time–pressure curve (Figure 1a, Step 4). If the actual pressure in the region is lower than the preloaded pressure curve, it sends the signal for a larger output to increase the pressure inside by a faster injection, and *vice versa*. This is the major difference from the previously developed CO_2-pressurized injector that provides sustained injection power output. To assess the controllability of this injector *in vitro*, various pressure curves—exponential (Figure 1b), convex (Figure 1c), stepwise (Figure 1d) and frequent spike (Figure 1e) pressure patterns—were preloaded into the system (gray solid lines in Figure 1), and hydrodynamic injections were performed into a specially constructed pressure-resistant reservoir connected to the HydroJector-EM. The actual pressure (black solid lines in Figure 1), and electromotor output power during the injections (black dotted lines in Figure 1) showed precise control of pressure and motor power over a short period, and even complex pressure patterns were precisely reproduced, suggesting a high level of controllability of the HydroJector-EM. This controllability of pressure during injection is important for reproducibility of an injection, as well as for safety in future human gene therapy, because it avoids unexpected too high pressure.

Pressure controllability of the HydroJector-EM *in vivo*

To examine whether the HydroJector-EM could reproduce the injection controllability *in vivo*, HGD was performed in rat livers using a catheter-based procedure (Figure 2). An injection catheter was inserted into the IVC and another catheter was placed in the PV close to the liver and was connected to a pressure sensor, which sent actual intrahepatic pressures to the programmed computer controlling the HydroJector-EM (Figure 2a). Using the same HydroJector-EM settings and various preloaded exponential time–pressure curves optimized *in vitro* (see Identification of the ideal time–pressure curves under Materials and methods section), pCMV-Luc plasmid solution in saline (5 μg ml^{-1}) was hydrodynamically injected into the whole liver. The representative time–pressure curves of i–iv are shown in Figure 2b. They were set to exponentially reach peak pressures of 15 mm Hg in 10 s (i), 15 mm Hg in 20 s (ii), 30 mm Hg in 10 s (iii) and 30 mm Hg in 20 s (iv) (see Materials and methods section). The actual intravascular pressures closely followed the preloaded computerized curves throughout the entire injection period (Figure 2c). The peak pressure achieved showed $<5\%$ delineation from the preloaded curves (for pressure i, actual pressure achieved 0.7 mm Hg higher than the preloaded 15 mm Hg), and the differences in injection volume between each animal injected with the same time–pressure curve were $<0.47\%$ BW (Figure 2d). These data support the high controllability of the HydroJector-EM *in vivo* using catheter-based procedure, resulting in reproducible hydrodynamic injection by replicating the time–pressure curves.

Efficiency and reproducibility of the HydroJector-EM-mediated gene delivery

The above time–pressure curves, using a manual injection method as a control, were completed safely, and liver, heart, lung and kidney tissues were harvested 3 h after the injections. The injection volume and time period for manual injection was set to be the same as curve iii with sustained injection flow rate showing a simple linear proportional time–pressure curve. The highest level of luciferase expression of 272 pg luciferase per mg of extracted proteins was obtained with pressure curve iii. This was 2–20 times higher than the levels achieved with pressure curves i, ii and iv, and with manual injection ($P<0.05$ for 'manual vs iii', but $P<0.01$ for 'iv vs iii' and $P<0.001$ for 'ii vs iii' and 'iv vs iii'; Figure 3a). No luciferase activity was detected in the heart, lung and kidneys (data not shown). Immunohistochemical staining using an anti-luciferase antibody was performed on livers collected 3 h after injection with pressure curves (Figures 3b–g). The largest number of the positively stained cells, 12.6%, was obtained with pressure curve iii, and was significantly 2.6–10 times higher than the levels achieved with pressure curves i, ii and iv ($P<0.001$ for 'i vs iii', 'ii vs iii' and 'iv vs iii'; Figure 3h). The level was

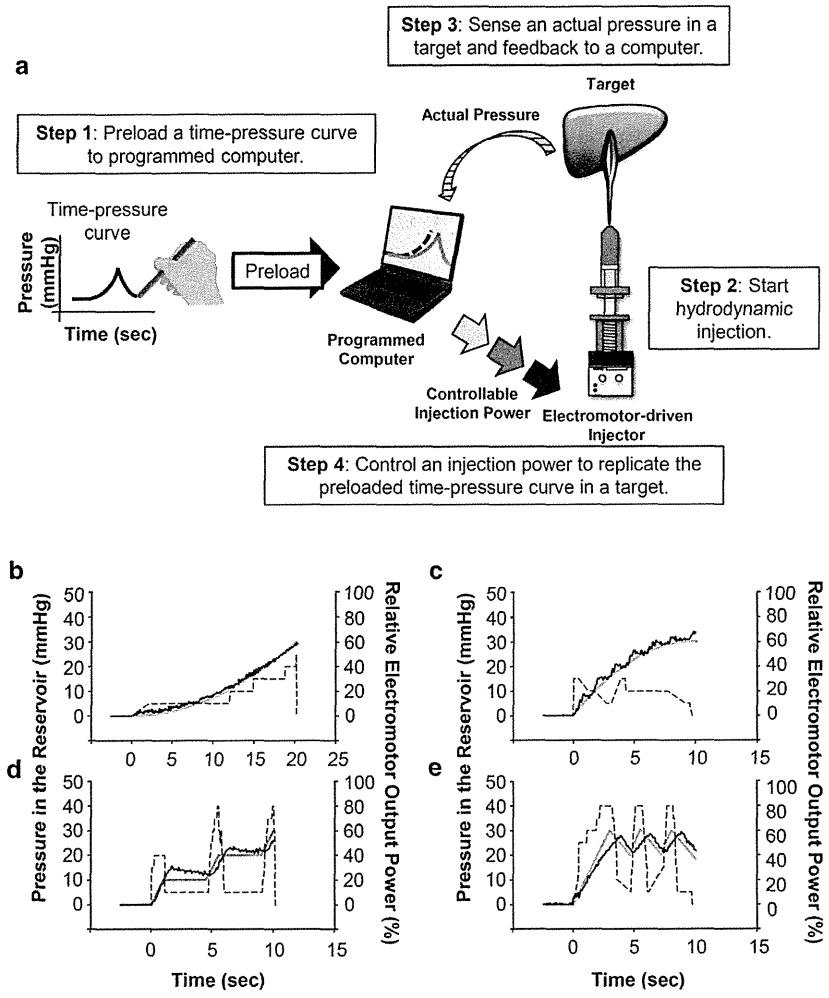

Figure 1. Development of the HydroJector-EM. Various time–pressure curves can be preloaded to the programmed computer. The electric power-driven injector injects a solution hydrodynamically by pushing the sterilized syringe. The actual pressure in the target during the injection is transmitted to the programmed computer every 0.05 s upon the injection through a sensor and amplifier. According to the actual pressure, the programmed computer controls the output electric-injection power moving to reproduce this preloaded pressure in the target region (**a**). Assessment of the controllability of the HydroJector-EM *in vitro* using a pressure-resistant reservoir connected to the HydroJector-EM (**b**–**e**). The exponential (**b**), convex (**c**), stepwise (**d**) and frequent spike (**e**) time–pressure patterns were preloaded to the system and tested for the reproducibility. Gray solid lines, black solid lines and black dotted lines represent time-dependent preloaded pressure, actual *in vitro* pressure and relative electromotor output power to its capacity, respectively.

not significantly different from the 10% positive cells obtained with manual injection (Figure 3h). These results suggest efficient and reproducible gene delivery by the HydroJector-EM and that pressure curve iii, which injects with a higher pressure over a shorter period, resulting in a more efficient gene delivery.

Physiological impacts

To examine the safety of our system, hematoxylin and eosin staining on the liver tissue and serum biochemical analysis were performed. The pressure curve iii injection, which achieved highest pressure over the shortest time among those tested, was compared with manual injection. Hematoxylin and eosin staining was performed on the liver tissues before (Figure 4a), immediately after (Figures 4b, c) and 3 h after (Figures 4d, e) the HydroJector-EM controlled injection with preloaded time–presure curve iii (Figures 4b, d) and manual injection (Figures 4c, e). There was a marked enlargement of the central veins and sinusoidal structure immediately following the injections (Figures 4b, c), and there were no marked differences between the injections. These enlargements recovered by 3 h post-injection, and no marked destruction of hepatocytes or necrotic tissues were seen 7 days after the injection (Figure 4f).

Blood samples were collected from the catheter placed in the IVC at the same time points as for the hematoxylin and eosin assays, and markers of liver status, including aspartate aminotransferase (AST), alanine aminotransferase (ALT) and lactate dehydrogenase (LDH) in the serum, were analyzed to assess tissue damage after injection with pressure curve iii and manual injection (Figures 4g, h). AST, ALT and LDH showed peak levels of 1418, 911 and 6671 IU ml^{-1}, respectively, 1 h after injection with pressure curve iii and 1228, 932 and 9065 IU ml^{-1}, respectively, 1 h after manual injection. These levels returned to normal 7 days after both injections, and no significant differences were seen. These results suggest that there are no significant differences in the physiological impact of computer-controlled and manual injections. These results also indicate that the HydroJector-EM can achieve efficient, reproducible and safe gene delivery *in vivo*.

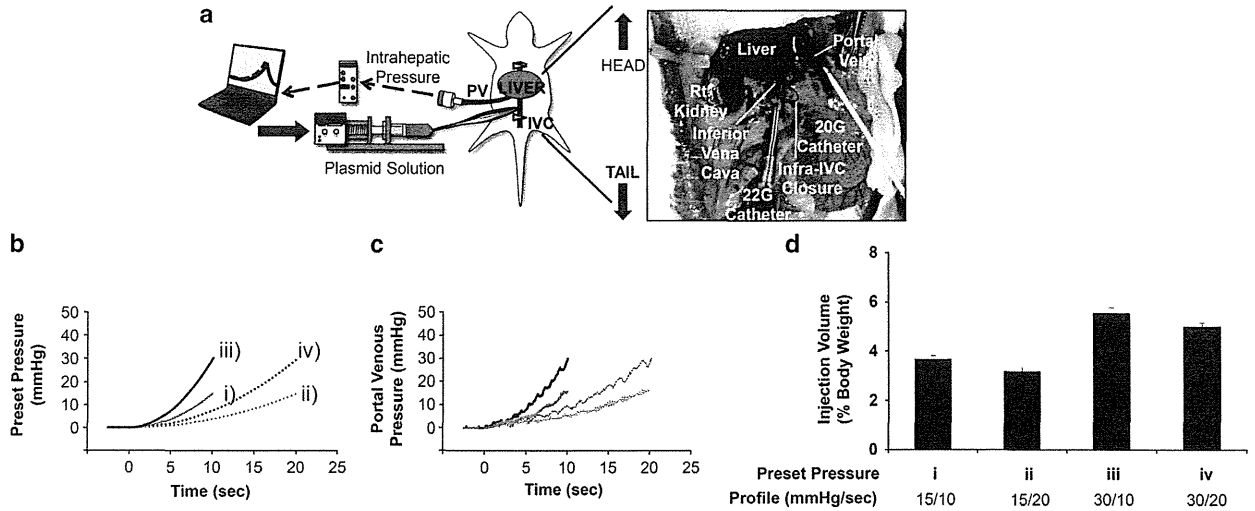

Figure 2. Pressure controllability of the HydroJector-EM in rat liver. (**a**) A pressure transducer was connected to a catheter (20 G) placed in the PV. Intravascular pressure was transmitted from the catheter to the computer controlling the electric power-driven gene injector. The injection catheter (22 G) was placed *via* the IVC of a rat (200 g) at the junction of the IVC and the hepatic veins followed by an injection of plasmid solution under temporal blood flow occlusions at the supra- and infrahepatic IVC. Various time–pressure curves were examined in rat liver to test whether intravascular pressure can be precisely controlled by the HydroJector-EM *in vivo*. (**b**) Time–pressure curves tested (peak pressure/injection period): i, gray solid line, 15 mm Hg/10 s; ii, gray dotted line, 15 mm Hg/20 s; iii, black solid line, 30 mm Hg/10 s; iv, black dotted line, 30 mm Hg/20 s. (**c**) Time-dependent actual portal venous pressures during the HydroJector-EM-controlled hydrodynamic injection. (**d**) The averages of injected volumes for pressure curves i–iv. The values represent mean ± s.d. ($n = 3$ for each curve).

Long-term gene expression study

Based on the above results, the pBS-HCRHP-FIXIA plasmid was hydrodynamically injected into rats using the HydroJector-EM, to examine the reproducibility of sustained gene expression. Pressure curve iii, which resulted in the highest gene delivery efficiency in the previous section, was utilized for the study, and the serum level of human factor IX was analyzed by enzyme-linked immunosorbent assay for 112 days. Additionally, injection using pressure curve i reaching 15 mm Hg and manual injection of 6% BW were tested for the same period. Human factor IX achieved its highest level of 5390 ± 474 ng ml^{-1} 7 days after injection with pressure curve iii. This was 17-fold higher than the level achieved with pressure curve i (317 ± 37 ng ml^{-1}; $P<0.001$) and 2.7-fold higher than the level achieved by manual injection (2030 ± 374 ng ml^{-1}; $P<0.01$). Human factor IX slowly decreased to the background level by 80 days after injection. Immunohistochemical staining using anti-human factor IX antibody was performed to confirm the results. Positively stained hepatocytes were detected 7 days after the injections (Figure 5, black arrows). Pressure curve iii injection resulted in 9.7% positively stained cells in four different sections (Figure 5d), whereas manual injection (Figure 5e) and injection with curve i (Figure 5c) resulted in 7.4% and 5.5% positive cells, respectively, while no stained cells were seen in saline-injected rats liver (Figure 5b). In addition, the level returned to this control level 112 days after the injection. Altogether, these data suggest that the HydroJector-EM gene transfer protocol can deliver plasmids safely and efficiently, and achieve a therapeutic level of human factor IX protein (>500 ng ml^{-1}) sustained for 2 months.

DISCUSSION

The list of applications for gene therapy is growing rapidly, including cancer, heart disease and hemophilia.[1] Among the various gene delivery methods, HGD is relatively new,[7] having first been reported by Liu *et al.*[2] and Zhang *et al.*[3] in 1999 as a simple and efficient gene delivery method through the tail veins of small animals. The key aspects for successful HGD include injection power, intravascular pressure, volume, speed and time period.[9–12] Various modifications have been made to the original procedure to apply this method to human gene therapy. The catheter-based procedure contributed to the reduction of injection volume[13–19] and the CO_2-pressurized injection device, the HydroJector, maintained injection parameters, such as sustained injection power, volume, speed and period for examining the optimum parameters for gene delivery efficiency and safety in large animals.[20] We have proven that the combination of these developments have achieved liver lobe- and target muscle-specific gene delivery in large animal and called 'Image-guided regional HGD'.[17,18] To further extend the clinical applicability of our technology, we have focused on the gene injection time–intravascular pressure curves to ensure the reproducibility and controllability of gene delivery in this study and developed a new electric power-driven injector, the HydroJector-EM. We have demonstrated that: (1) it can precisely replicate the time–pressure curves preloaded into the system before HGD in animals and ensure reproducible gene delivery to various targets by flexibly changing the electric-injection power; (2) it consists of clinically approved parts and disposable products; and (3) it utilizes electric power as a physical force for HGD rather than the CO_2 gas used in previous studies, thereby reducing the risk of gas embolism (although this small amount of CO_2 gas is also used for phase contrast in angiography with patients who have allergies to contrast enhancements).

The HydroJector-EM showed efficient gene delivery with time–pressure curve iii reaching 30 mm Hg in 10 s, which was the highest pressure over the shortest period among tested. The level of luciferase expression was higher than the manual injection utilizing the same volume and period, probably due to the difference in pressure–time curves, 'exponential' with iii and simple 'linear proportional line' with fixed flow rate manual injection. However, the manual injection also achieved the therapeutic level of hFIX, although lower level than curve iii, the proximity of the efficacy of both procedures was revealed. The significant advantage of our injector and the difference from

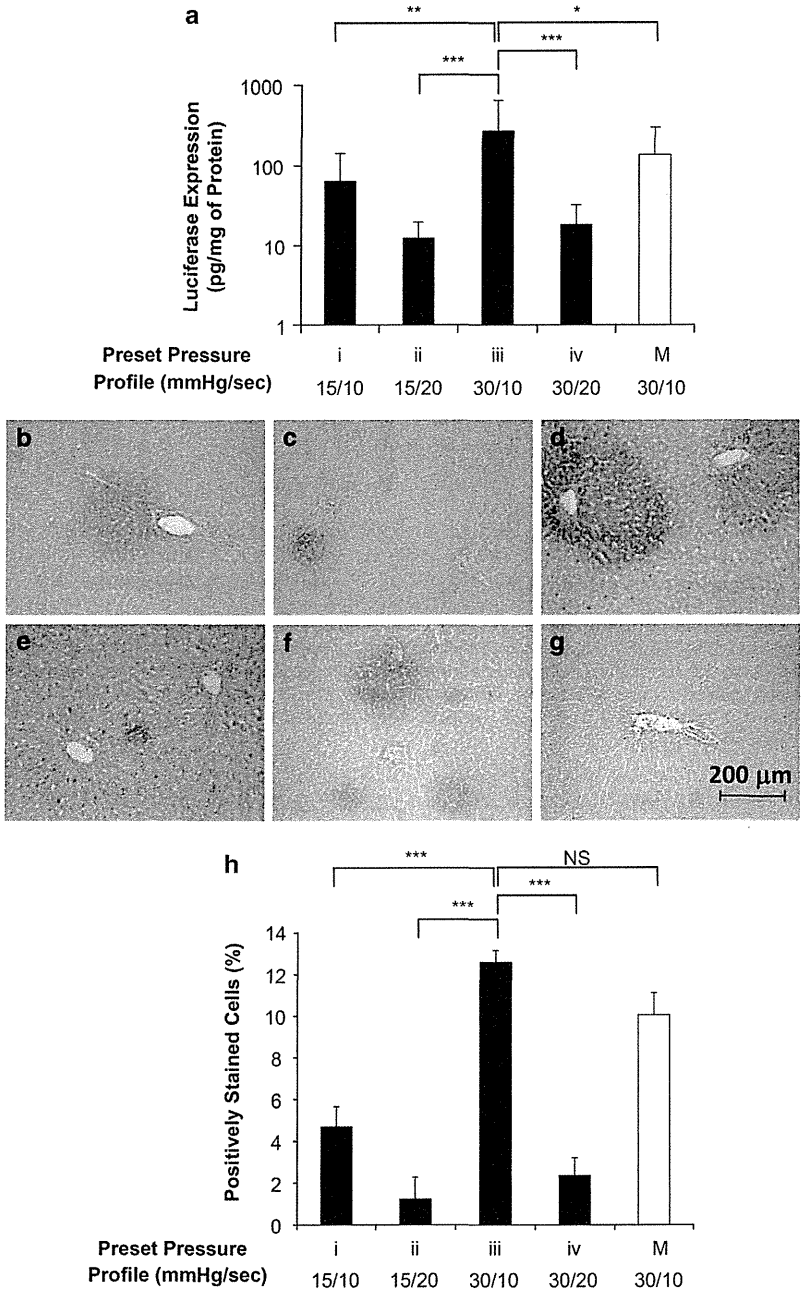

Figure 3. Gene delivery efficiency in rat liver. (**a**) A total of 12 rats received an injection of pCMV-Luc plasmid DNA using preloaded time–pressure curves shown in Figure 2b, and were euthanized 3 h later for tissue analysis of luciferase expression. Manual injection (M) with a volume of 6% BW in 10 s was performed as a control in three rats. The values represent mean ± s.d. (five samples from every liver lobe per rat from all three rats in each group, 15 samples for each curve and manual injection). Immunohistochemical (IHC) staining with anti-luciferase antibody was performed on liver tissues collected (**b**–**f**). Scale bar represents 200 µm (× 100). (**b**) Injected with curves of i; (**c**) ii; (**d**) iii; (**e**) iv; (**f**) manual injection; and (**g**) untreated animals. (**h**) Quantitative analysis of positively stained cells. Four different liver sections from three rats in each group and untreated rats were immunohistochemically stained with anti-luciferase antibody and a quantitative analysis was performed using the ImageJ software (version 1.6.0_20; National Institutes of Health). The values represent mean ± s.d. for $^{*}P<0.05$, $^{**}P<0.01$, $^{***}P<0.001$ and NS, no statistical significance. One-way analysis of variance (ANOVA) followed by Bonferroni's multiple comparison test.

the manual injection is that the reproducibility of our injection showing the less variability of gene expression in animals (Supplementary Figure S1). Since the gene delivery efficiency by the sustained flow rate injection by manual or single pump was affected by the possible leakage due to the intravenous anastomosis in large animals and the high intravascular pressure due to the species specific structure of target organ tissue, such as fibrotic tissue in pigs liver, this reproducibility achieved by the HydroJector-EM, that flexibly control the injection power, will exceed these matters and be efficient in the gene delivery in various large animals because the injection power changes according to the actual intravascular pressure upon the injection. The serum levels of AST, ALT and LDH reached peak in 1 h after the injection as reported previously,[12] with a traditional tail vein

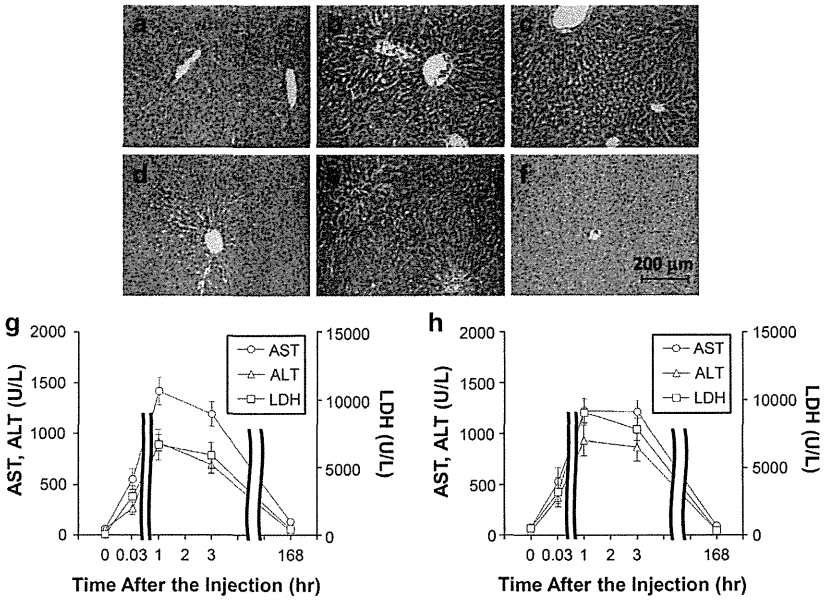

Figure 4. Physiological impacts in rats. Hematoxylin and eosin (HE) staining was performed on the liver tissue before (**a**), immediately after (**b, c**), 3 h (**d, e**) and 7 days after the HydroJector-EM controlled injection with time–pressure curve iii (**b, d, f**) and manual injection (**c, e**). Scale bar represents 200 μm (× 100). Blood biochemical analyses after the injections with pressure curve iii (**g**) and manual injection (**h**). Blood samples were collected from the catheter placed in the IVC before (time = 0), 2 min, 1 h, 3 h and 7 days after the injections. The values represent average of AST, ALT and LDH in the serum ($n = 3$ from each group). Open circular, triangular, square markers represent AST, ALT and LDH, respectively. The values represent mean ± s.d.

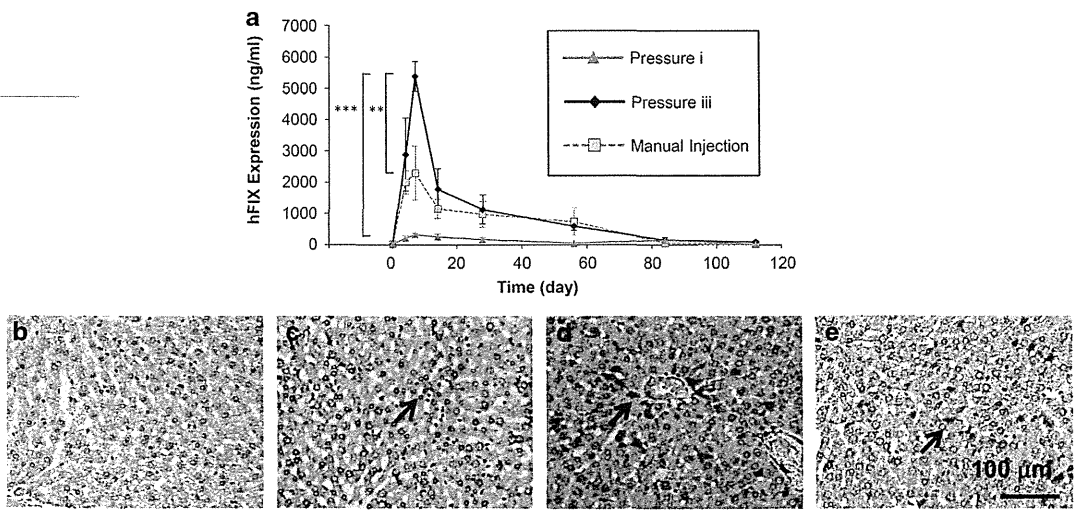

Figure 5. Long-term gene expression in rat liver. (**a**) Plasma concentrations of human factor IX. Blood samples were collected before, 4, 7, 14, 28, 56, 84 and 112 days after the hydrodynamic injection of human factor IX expressing plasmid DNA with pressure curves i and iii, and manual injection. Enzyme-linked immunosorbent assay was performed on those samples using a mouse anti-hFIX monoclonal antibody for plate coating, and the horse radish peroxidase-conjugated goat anti-hFIX polyclonal antibody. The values represent mean ± s.d. ($n = 3$ for each group). (**b**–**e**) Liver tissues were collected 7 days after the injection and IHC was performed with rabbit anti-hFIX polyclonal antibody (**b**, saline injected with curve of iii; **c**, plasmid injected with curve i; **d**, iii; **e**, manual). Scale bar represents 100 μm (× 200). Black arrows represent positively stained cells. $^{**}P < 0.01$, $^{***}P < 0.001$. Two-way factor repeated-measure analysis of variance (ANOVA) test followed by Bonferroni test. Gray solid line with gray triangular markers, black solid line with black diamond-shaped markers and gray dotted line with gray square markers represent hFIX concentration with pressure curve i, iii and manual injection.

injection of 7.5% BW volume. The level was 10-fold higher than that achieved by the tail vein injection,[12] probably due to the difference in injection site since our catheter-based procedure directly injects to the whole liver with temporal blood flow occlusion at IVC to reduce the injection volume.

Our long-term study showed a promising therapeutic level of hFIX expression that was sustained for more than 2 months. The level achieved was comparable to the results shown in previous studies by Miao's group[21–23] using mouse tail vein injection and ultrasound. For hemophilia gene therapy, a number of studies, especially those using an adeno-associated virus vector, have shown therapeutic and sustained hFIX expression in animals (for recent reviews, see Tuddenham[24] and Benveniste[25]). Interestingly, Brunetti-Pierri *et al.*[26] utilized a catheter-based procedure for

helper-dependent adenoviral vector transfer to the monkey liver and showed increased liver-specific transduction showing therapeutic level of gene expression with reduced systemic vector dissemination, suggesting the importance of a catheter-based procedure. While viral vectors are highly effective and have been used in quite a few clinical trials, the intrinsic carcinogenesis- and immune-response-stimulating properties of viral genomes and proteins remain the largest hurdle, and the injection of plasmid DNA is considered to be safer.[7] Therefore, the results obtained in this study suggest a promising option for hemophilia gene therapy, as the automatic-injector delivery of simple naked DNA achieved a therapeutic level that has never before been seen in rats. The slow decrease to the background level by 80 days after injection was probably due to factors, such as methylation of plasmid,[27] antibody to the human factor IX.[28]

In addition, the reproducible gene delivery efficiency based on the intravascular time–pressure curve may enable us to estimate the therapeutic effect upon gene delivery, and this new system suggests versatile applications, including combining with virus vector and protein delivery, among other possibilities.[9,20]

In summary, we have reported on the development and effectiveness of the HydroJector-EM. We have confirmed its reproducibility and controllability for gene delivery and long-term therapeutic gene expression. An assessment of its effectiveness in large animals, organs and disease models combined with a catheter-based procedure will be the next logical steps toward clinical applications. The fine-tuning of the procedure and plasmid engineering is also a necessary prerequisite for clinical trials of HGD.

MATERIALS AND METHODS

Materials

The pCMV-Luc plasmid containing firefly luciferase cDNA driven by a CMV promoter was purified by the method of CsCl-ethidium bromide gradient centrifugation and kept in a Tris-EDTA buffer. The pBS-HCRHP-FIXIA plasmid containing human factor IX gene driven by hAAT promoter was kindly provided by Dr Carl Miao's lab.[22] The purity of the plasmid preparation was checked by absorbency at 260 and 280 nm and 1% agarose gel electrophoresis. The luciferase assay kit was from Wako Pure Chemical Industries Ltd (Chuo-ku, Osaka, Japan). The electric power-driven motor for the injector was from Tsugawa EW Co. Ltd (Nishinari-ku, Osaka, Japan). The pressure transducer was from Kyowa Electronic Instruments Co. Ltd (Chofu, Tokyo, Japan). The charger amplifier unit AG3101 was from NEC Avio Infrated Technologies Co. Ltd (Shinagawa-ku, Tokyo, Japan). Wistar rats (female, 150–200 g) were purchased from Japan SLC Inc. (Hamamatsu, Shizuoka, Japan).

Hydrodynamic injection into rat liver

All animal experiments were conducted in full compliance with regulation and approved by the Institutional Animal Care and Use Committee at the Niigata University (Niigata, Japan). A midline skin incision was made under general anesthesia using isoflurane and 2,2,2-tribromoethanol (concentration, 0.016 g ml^{-1} in 0.9% saline; dose, 1.25 ml/100 g BW). With a small incision in the abdominal wall, an injection catheter (SURFLO 22 gauge; Terumo, Sibuya-ku, Tokyo, Japan) was inserted *via* the IVC and its tip placed at the junction of the IVC and the hepatic veins. A pressure transducer was connected to another catheter (SURFLO 20 gauge; Terumo) placed in the PV in hepatic hilar side, which reflected the intrahepatic sinusoidal pressure upon the injection.[29] Saline containing either pCMV-Luc or pBS-HCRHP-FIXIA plasmid DNA (5 μg ml^{-1}) was injected into the liver *via* the HydroJector-EM under the program with temporal blood flow occlusions at the supra- and infrahepatic IVC as used in small animals[20] and in non-human primates.[26,30] The incision made at the animals' abdomen was sutured after the procedure.

Identification of the ideal time–pressure curves

HGD was performed in rats with different settings of preloaded exponential time–pressure curves. Among the various pressure curves tested *in vitro* shown in Figure 1, exponential curves with a peak pressure of 15 and 30 mm Hg and injection period of 10 and 20 s were chosen for the gene delivery analysis since the other curves with higher pressure and longer period showed intolerableness in rats cardiovascular condition.

Manual injection procedure

To examine the safety and efficiency of the HydroJector-EM controlled injections, the steady manual injection of 6% BW, the same volume as used in pressure curve iii (5.5 ± 0.47%) in 10 s was performed.

Lucierase assay

HGD of pCMV-Luc plasmid DNA was performed with different settings of preloaded time–pressure curves. The rat was euthanized 3 h after the injection of pCMV-Luc plasmid DNA and tissue samples were collected from each lobe of the liver, kidney, lung and heart. Tissue samples for the luciferase assay were kept in −80 °C until use. A measure of 1 ml of lysis buffer (0.1 M Tris–HCl, 2 mM EDTA and 0.1% Triton X-100, pH 7.8) was added to each sample (~200 mg) and the samples were homogenized for 30 s with the tissue homogenizer (ULTRA-TURRAX T25 Digital; IKA, Staufen, Germany) at maximum speed. The tissue homogenates were centrifuged in a microcentrifuge for 10 min at 13 000 *g* at 4 °C. The protein concentration of the supernatant was determined by Protein Assay Kit (Bio-Rad, Hercules, CA, USA) based on Coomassie blue assay strategy. A measure of 10 μl of supernatant was mixed with 100 μl of luciferase assay reagent and the luciferase activity was measured in a luminometer (Luminescencer Octa AB-2270; Atto, Bunkyo-ku, Tokyo, Japan) for 10 s according to the previously established procedure.[2] Luciferase activity obtained as the relative light units was converted to luciferase mass using standard curve established using reagents and procedure from Analytic Luminescence Laboratory (San Diego, CA, USA).[2] The amount of luciferase protein in the tissue extract was calculated using the equation derived from the standard curve in which luciferase protein (pg) = 7.98 × 10^{-5} RLU + 0.093 (R^2 = 0.9999).[2]

Analysis of serum hFIX concentration

Animals were hydrodynamically injected with the pBS-HCRHP-FIXIA plasmid or saline. Blood samples were collected from their tail vein before, 4, 7, 14, 28, 56, 84 and 112 days after the gene delivery according to the preliminary data and plasma were collected for enzyme-linked immunosorbent assay. A mouse anti-hFIX monoclonal antibody (clone HIX-1, F2645l Sigma, St Louis, MO, USA) was used for plate coating, and the horse radish peroxidase-conjugated goat anti-hFIX polyclonal antibody (GAFIX-HRP; Affinity Biologicals, Ancaster, ON, Canada) was used as the second antibody for binding to hFIX that bound to the well.

Immunohistochemical stainings

Tissue samples for immunohistochemical stainings were collected 3 h after the injection for luciferase staining and 7 and 112 days after for hFIX staining. Four different liver sections from three rats in each group and untreated rats were immunohistochemically stained with anti-luciferase antibody or anti-hFIX antibody. Tissues were fixed in 10% formalin upon the collection and embedded in paraffin. Sections (10 μm) were made and standard immunohistochemistry was performed with a goat anti-luciferase polyclonal antibody (G7451, 1:50 dilution; Promega, Madison, WI, USA), Vecstatin Elite ABC Goat IgG Kit (PK-6105; Vector Laboratories Inc., Burlingame, CA, USA) and DAB chromogen tablet (Muto Pure Chemicals Co. Ltd, Bunkyo-ku, Tokyo, Japan) for luciferase staining. The rabbit anti-hFIX polyclonal antibody (HPA 000254, 1:100 dilution; Sigma), Vecstatin Elite ABC Rabbit IgG Kit (PK-6101; Vector Laboratories Inc.), and DAB chromogen tablet (Muto Pure Chemicals Co. Ltd) were used for hFIX staining.

Every three fields from each section (total of 36 fields for each curves and control) were captured and a quantitative analysis of positively stained cells was performed using the ImageJ software (version 1.6.0_20; National Institutes of Health, Bethesda, MD, USA) as previously reported method.[31]

Assessment of tissue damages

The blood samples were collected at the appropriate time points as in the previous study,[12] which were before (time = 0), 2 min, 1 h and 3 h after the hydrodynamic injection of pCMV-Luc from seven animals and additional data points before, 2 min and 7 days after the injection were collected from nine rats hydrodynamically injected with pBS-HCRHP-FIXIA. Automated concentration determination of ALT, AST and LDH was performed by BML

Inc. (Shibuya-ku, Tokyo, Japan). The liver tissue samples collected 3 h after the injection were analyzed by hematoxylin and eosin staining.

Statistical methods

The luciferase and enzyme-linked immunosorbent assay assays were statistically evaluated by analysis of variance followed by Bonferroni's multiple comparison test.

CONFLICT OF INTEREST

The authors declare no conflict of interest.

ACKNOWLEDGEMENTS

This work was supported in part by JSPS Grants 22890064, 23790595, The Sumitomo Foundation Grant 100033 and Takeda Science Foundation Grant to KK. The authors acknowledge Takao Tsuchida, Division of Gastroenterology and Hepatology, Niigata University, for his excellent assistance for histological stainings. The authors would like to thank Nobuyoshi Fujisawa, Minoru Tanaka and all staff members in Division of Laboratory Animal Resources in Niigata University for the excellent assistance for animal care. We thank Enago for the English language review.

REFERENCES

1 The Journal of Gene Medicine. Gene therapy clinical trials worldwide. http://www.wiley.com/legacy/wileychi/genmed/clinical/ (accessed on 28 August 2012).
2 Liu F, Song Y, Liu D. Hydrodynamics-based transfection in animals by systemic administration of plasmid DNA. *Gene Therapy* 1999; **6**: 1258–1266.
3 Zhang G, Budker V, Wolff JA. High levels of foreign gene expression in hepatocytes after tail vein injections of naked plasmid DNA. *Hum Gene Ther* 1999; **10**: 1735–1737.
4 Suda T, Liu D. Hydrodynamic gene delivery: its principles and applications. *Mol Ther* 2007; **15**: 2063–2069.
5 Herweijer H, Wolff JA. Gene therapy progress and prospects: hydrodynamic gene delivery. *Gene Therapy* 2007; **14**: 99–107.
6 Kamimura K, Liu D. Physical approaches for nucleic acid delivery to liver. *AAPS J* 2008; **10**: 589–595.
7 Kamimura K, Suda T, Zhang G, Liu D. Advances in gene delivery systems. *Pharm Med* 2011; **25**: 293–306.
8 Bonamassa B, Hai L, Liu D. Hydrodynamic gene delivery and its applications in pharmaceutical research. *Pharm Res* 2011; **28**: 694–701.
9 Suda T, Gao X, Stolz DB, Liu D. Structural impact of hydrodynamic injection on mouse liver. *Gene Therapy* 2007; **14**: 129–137.
10 Zhang G, Song YK, Liu D. Long-term expression of human alpha1-antitrypsin gene in mouse liver achieved by intravenous administration of plasmid DNA using a hydrodynamics-based procedure. *Gene Therapy* 2000; **7**: 1344–1349.
11 Zhang G, Gao X, Song YK, Vollmer R, Stolz DB, Gasiorowski JZ *et al.* Hydroporation as the mechanism of hydrodynamic delivery. *Gene Therapy* 2004; **11**: 675–682.
12 Zhou T, Kamimura K, Zhang G, Liu D. Intracellular gene transfer in rats by tail vein injection of plasmid DNA. *AAPS J* 2010; **12**: 692–698.
13 Eastman SJ, Baskin KM, Hodges BL, Chu Q, Gates A, Dreusicke R *et al.* Development of catheter-based procedures for transducing the isolated rabbit liver with plasmid DNA. *Hum Gene Ther* 2002; **13**: 2065–2077.
14 Yoshino H, Hashizume K, Kobayashi E. Naked plasmid DNA transfer to the porcine liver using rapid injection with large volume. *Gene Therapy* 2006; **13**: 1696–1702.
15 Alino SF, Herrero MJ, Noguera I, Dasi F, Sanchez M. Pig liver gene therapy by noninvasive interventionist catheterism. *Gene Therapy* 2007; **14**: 334–343.
16 Fabre JW, Grehan A, Whitehorne M, Sawyer GJ, Dong X, Salehi S *et al.* Hydrodynamic gene delivery to the pig liver via an isolated segment of the inferior vena cava. *Gene Therapy* 2008; **15**: 452–462.
17 Kamimura K, Suda T, Xu W, Zhang G, Liu D. Image-guided, lobe-specific hydrodynamic gene delivery to swine liver. *Mol Ther* 2009; **17**: 491–499.
18 Kamimura K, Guisheng Z, Liu D. Image-guided, intravascular hydrodynamic gene delivery to skeletal muscle in pigs. *Mol Ther* 2010; **18**: 93–100.
19 Herrero MJ, Sabater L, Guenechea G, Sendra L, Montilla AI, Abargues R *et al.* DNA delivery to '*ex vivo*' human liver segments. *Gene Therapy* 2012; **9**: 504–512.
20 Suda T, Suda K, Liu D. Computer-assisted hydrodynamic gene delivery. *Mol Ther* 2008; **16**: 1098–1104.
21 Miao CH, Thompson AR, Loeb K, Ye X. Long-term and therapeutic-level hepatic gene expression of human factor IX after naked plasmid transfer *in vivo*. *Mol Ther* 2001; **3**: 947–957.
22 Miao CH, Ye X, Thompson AR. High-level factor VIII gene expression *in vivo* achieved by nonviral liver-specific gene therapy vectors. *Hum Gene Ther* 2003; **14**: 1297–1305.
23 Miao CH, Brayman AA, Loeb KR, Ye P, Zhou L, Mourad P *et al.* Ultrasound enhances gene delivery of human factor IX plasmid. *Hum Gene Ther* 2005; **16**: 893–905.
24 Tuddenham E. Gene therapy for haemophilia B. *Haemophilia* 2012; **18**(Suppl 4): 13–17.
25 Benveniste O. Gene therapy, an ongoing revolution. *Blood* 2012; **119**: 2973–2974.
26 Brunetti-Pierri N, Liou A, Patel P, Palmer D, Grove N, Finegold M *et al.* Balloon catheter delivery of helper-dependent adenoviral vector results in sustained, therapeutic hFIX expression in Rhesus macaques. *Mol Ther* 2012; **20**: 1863–1870.
27 Schuttrumpf J, Milanov P, Abriss D, Roth S, Tonn T, Seifried E. Transgene loss and changes in the promoter methylation status as determinants for expression duration in nonviral gene transfer for factor IX. *Hum Gene Ther* 2011; **22**: 101–106.
28 Scott DW, Lozier JN. Gene therapy for haemophilia: prospects and challenges to prevent or reverse inhibitor formation. *Br J Haematol* 2012; **156**: 295–302.
29 Vollmar B, Menger MD. The hepatic microcirculation: mechanistic contributions and therapeutic targets in liver injury and repair. *Physiol Rev* 2009; **89**: 1269–1339.
30 Brunetti-Pierri N, Stapleton GE, Law M, Breinholt J, Palmer DJ, Zuo Y *et al.* Efficient, long-term hepatic gene transfer using clinically relevant HDAd doses by balloon occlusion catheter delivery in nonhuman primates. *Mol Ther* 2009; **17**: 327–333.
31 Vrekoussis T, Chaniotis V, Navrozoglou I, Dousias V, Pavlakis K, Stathopoulos EN *et al.* Image analysis of breast cancer immunohistochemistry-stained sections using ImageJ: an RGB-based model. *Anticancer Res* 2009; **29**: 4995–4998.

Supplementary Information accompanies the paper on Gene Therapy website (http://www.nature.com/gt)

Gastric Cancer (2013) 16:208–219
DOI 10.1007/s10120-012-0172-3

ORIGINAL ARTICLE

Re-evaluation of phenotypic expression in undifferentiated-type early gastric adenocarcinomas using mucin core protein and CDX2

Satoshi Ikarashi · Ken Nishikura · Yoichi Ajioka · Yutaka Aoyagi

Received: 25 January 2012 / Accepted: 1 June 2012 / Published online: 25 July 2012

Abstract
Background Undifferentiated-type early gastric adenocarcinomas are generally classified into two groups: pure undifferentiated-type adenocarcinomas, which naturally develop as undifferentiated-type without a glandular component; and mixed differentiated/undifferentiated-type adenocarcinomas, which are associated with some vestigial glandular component and presumably develop from differentiated-type adenocarcinoma. The differences in phenotypic expression between these two groups were examined using mucin core protein and CDX2.
Methods A total of 210 lesions of undifferentiated-type early gastric adenocarcinoma less than 25 mm in diameter were classified into four categories (gastric type, gastrointestinal type, intestinal type, and null type) based on their MUC5AC, MUC6, MUC2, and CDX2 immunoprofiles.
Results Gastric type was significantly ($p < 0.01$) decreased and gastrointestinal type was significantly ($p < 0.01$) increased both in pure undifferentiated-type adenocarcinomas and in mixed differentiated/undifferentiated-type adenocarcinomas when CDX2 was applied to mucin core protein. In the pure undifferentiated-type adenocarcinomas, gastric type decreased and gastrointestinal type increased as tumor size increased ($p < 0.05$). In contrast, in the mixed differentiated/undifferentiated-type adenocarcinomas, gastrointestinal type was most common even in small-sized ($\leq$10 mm) carcinomas and was generally stable regardless of tumor size. In submucosal carcinomas, gastrointestinal type decreased and gastric type and intestinal type increased during carcinoma invasion from the intramucosal to submucosal parts ($p < 0.05$). The positivity rates for all phenotypic markers, especially gastric markers, tended to decrease during submucosal invasion.
Conclusions CDX2 is a sensitive marker for assessing intestinal phenotypic expression, and it is likely that there are two different pathways of tumor progression in undifferentiated-type adenocarcinoma of the stomach, according to phenotypic expression.

Keywords Early gastric adenocarcinoma · Undifferentiated-type · Phenotype · Mucin core protein · CDX2

S. Ikarashi and K. Nishikura contributed equally to this work.

S. Ikarashi · Y. Ajioka
Division of Molecular and Diagnostic Pathology, Niigata University Graduate School of Medical and Dental Sciences, Niigata, Japan

S. Ikarashi · Y. Aoyagi
Division of Gastroenterology and Hepatology, Niigata University Graduate School of Medical and Dental Sciences, Niigata, Japan

K. Nishikura (✉)
Division of Molecular and Functional Pathology, Niigata University Graduate School of Medical and Dental Sciences, 1-757 Asahimachi-dori, Chuo-ku, Niigata 951-8510, Japan
e-mail: knishi@med.niigata-u.ac.jp

Introduction

Histologically, human gastric adenocarcinomas have been classified into two major groups by Lauren [1]—the intestinal type and the diffuse type (depending on the degree of glandular formation of the cancer cells)—a classification which roughly corresponds to the differentiated type and undifferentiated type, respectively [2]. It has been considered that the differentiated types arise from

intestinalized mucosa and take an intestinal phenotype, while the undifferentiated types develop from atrophic gastric mucosa without intestinal metaplasia and take a gastric phenotype [3, 4]. This hypothesis is based on morphological similarities between cancers and intestinal metaplasia, as well as being based on the results of comparisons between carcinomas and the surrounding mucosa. However, recent advances in mucin immunohistochemistry, including mucin core protein (MUC), have revealed that differentiated-type adenocarcinomas are composed of both intestinal and gastric phenotypes [5–8].

Previous investigations of the phenotypic expression of undifferentiated-type adenocarcinomas are limited, and it has been reported that there are some undifferentiated-type adenocarcinomas of intestinal phenotype [9, 10], and that the intestinal phenotype in gastric signet-ring cell carcinomas appears to occur during tumor progression [11–13] or during tumor spread in the mucosa [14]. However, how frequent and when phenotypic alteration occurs during the development of undifferentiated-type adenocarcinomas remain controversial.

There are several commercial markers that are useful for distinguishing gastric carcinoma phenotypes. The caudal-related homeobox gene CDX2 is important for the maintenance of intestinal epithelial cells [15], and there have been several reports of CDX2 expression in human gastric carcinomas and intestinal metaplasia [16–20]. It has previously been shown that CDX2 is closely associated with intestinal phenotypic expression in gastric carcinomas [17–19, 21]. However, few studies have evaluated phenotypic expression in undifferentiated-type adenocarcinoma and/or signet-ring cell carcinoma using CDX2 as a phenotypic marker [16, 17, 22, 23].

It has been reported that, as gastric adenocarcinoma invades deeply or increases in size, the incidence of differentiated-type decreases and that of undifferentiated-type increases [24–26], which raises the possibility of histological transformation from differentiated-type to undifferentiated-type during tumor progression. Furthermore, differentiated-type adenocarcinomas of the gastric phenotype are considered to have higher rates of histological transformation into undifferentiated-type adenocarcinomas, as well as higher biological malignancy, such as high invasiveness and high metastatic potential, compared with those of the intestinal phenotype [27]. In contrast, even minute gastric adenocarcinomas, up to 5 mm in size and considered to be incipient in carcinogenesis, contain a certain amount of pure undifferentiated-type adenocarcinoma. These findings allow us to postulate different development pathways for undifferentiated-type adenocarcinoma: one that naturally develops as undifferentiated-type without a glandular component (pure undifferentiated-type: PURE-type); and one that develops with some rudimentary glandular component (mixed undifferentiated-type and differentiated-type: MIXED-type), presumably from differentiated-type adenocarcinoma.

The aim of this study was to clarify the differences in phenotypic expression between these two groups of undifferentiated-type adenocarcinomas: PURE-type carcinoma and MIXED-type carcinoma. For this purpose, (1) two different criteria of phenotypic classification were compared (immunoprofile based on MUC only and that based on MUC and CDX2 combined), and (2) differences in phenotypic expression between PURE-type carcinoma and MIXED-type carcinoma were examined according to the background mucosa, depth of tumor invasion, and tumor size.

Materials and methods

Patients, lesions, and tissue sampling

From our pathological files of gastric carcinomas from July 1979 through March 2006, 210 lesions of undifferentiated-type early gastric adenocarcinomas measuring less than 25 mm in diameter were selected for this study. All tumors had been surgically resected, from 203 Japanese patients who had had no systemic adjuvant therapy, at Niigata University General Hospital and its affiliated institutions. Each surgically resected specimen was fixed in 10 % buffered neutral formalin solution and serially cut into 5-mm-thick sections throughout each lesion and embedded in paraffin. All sections were stained with hematoxylin–eosin (HE) for histological examination. Paraffin blocks corresponding to the selected HE sections were cut into 3-μm-thick consecutive sections for immunohistochemical staining.

The histological classification was based on the *Japanese classification of gastric carcinoma* [28]. Undifferentiated-type adenocarcinomas were defined as those with indistinct or no glandular structure, including solid-type, poorly differentiated adenocarcinoma (por1); non-solid-type, poorly differentiated adenocarcinoma (por2); and signet-ring cell carcinoma (sig). The undifferentiated-type adenocarcinomas were further subclassified into two groups: (1) PURE-type, without any glandular formation; and (2) MIXED-type, with a mixture of non-glandular (POR) and some vestigial glandular (TUB) components.

Immunohistochemical staining

For antigen retrieval, the deparaffinized sections were microwave-treated at approximately 98 °C for 20 min (sections for MUC5AC/HGM, MUC6, MUC2, and CDX2) in 10 mmol/L citrate buffer (pH 6.0, except for

sections for CDX2), and in 1 mmol/L tris–ethylenediamine tetraacetic acid buffer (pH 9.0, sections for CDX2). Endogenous peroxidase activity was blocked by 20 min of incubation with 0.3 % hydrogen peroxidase in absolute methanol, and then the sections were washed in tap water. Non-specific binding was blocked with normal serum (Nichirei, Tokyo, Japan). The sections were incubated overnight with monoclonal antibodies as follows: (1) MUC5AC (CLH2, 1:100 dilution; Novocastra Laboratories, Newcastle, UK) and/or HGM (45M1, 1:50; Novocastra) as a marker for gastric foveolar epithelium; (2) MUC6 (CLH5, 1:100; Novocastra) and/or M-GGMC-1 (HIK 1083, 1:50; Kanto Chemical, Tokyo, Japan) as a marker for pyloric glands; and (3) MUC2 (Ccp58, 1:300; Novocastra) and CDX2 (AMT28, 1:100; Novocastra) as markers for goblet cells and intestinal epithelial cells. The sections were then incubated with Histofine Simple Stain MAX-PO (MULTI) (Nichirei Biosciences , Tokyo, Japan) for 30 min at room temperature. Antibody-antigen reactivity was visualized using diaminobenzidine and light counterstaining with hematoxylin.

Definition of phenotypes of carcinomas

MUC5AC, HGM, MUC6, and M-GGMC-1 were defined as gastric phenotype markers, whereas MUC2 and CDX2 were selected as intestinal phenotype markers. It has been reported that MUC5AC and MUC6 recognize core proteins, whereas HGM and M-GGMC-1 recognize carbohydrate side-chains [8, 29–31]. Cytoplasmic reactivity was judged as positive for MUC5AC/HGM, MUC6/M-GGMC-1, and MUC2, and nuclear reactivity was judged as positive for CDX2. Samples were classified as positive if 5 % or more of the tumor cells were stained; otherwise they were considered negative [8, 16, 22]. Using these markers, the phenotypes were classified into four categories: (1) gastric type (G type), demonstrating positive expression for gastric markers but negative expression for intestinal markers (Fig. 1); (2) intestinal type (I type), demonstrating positive

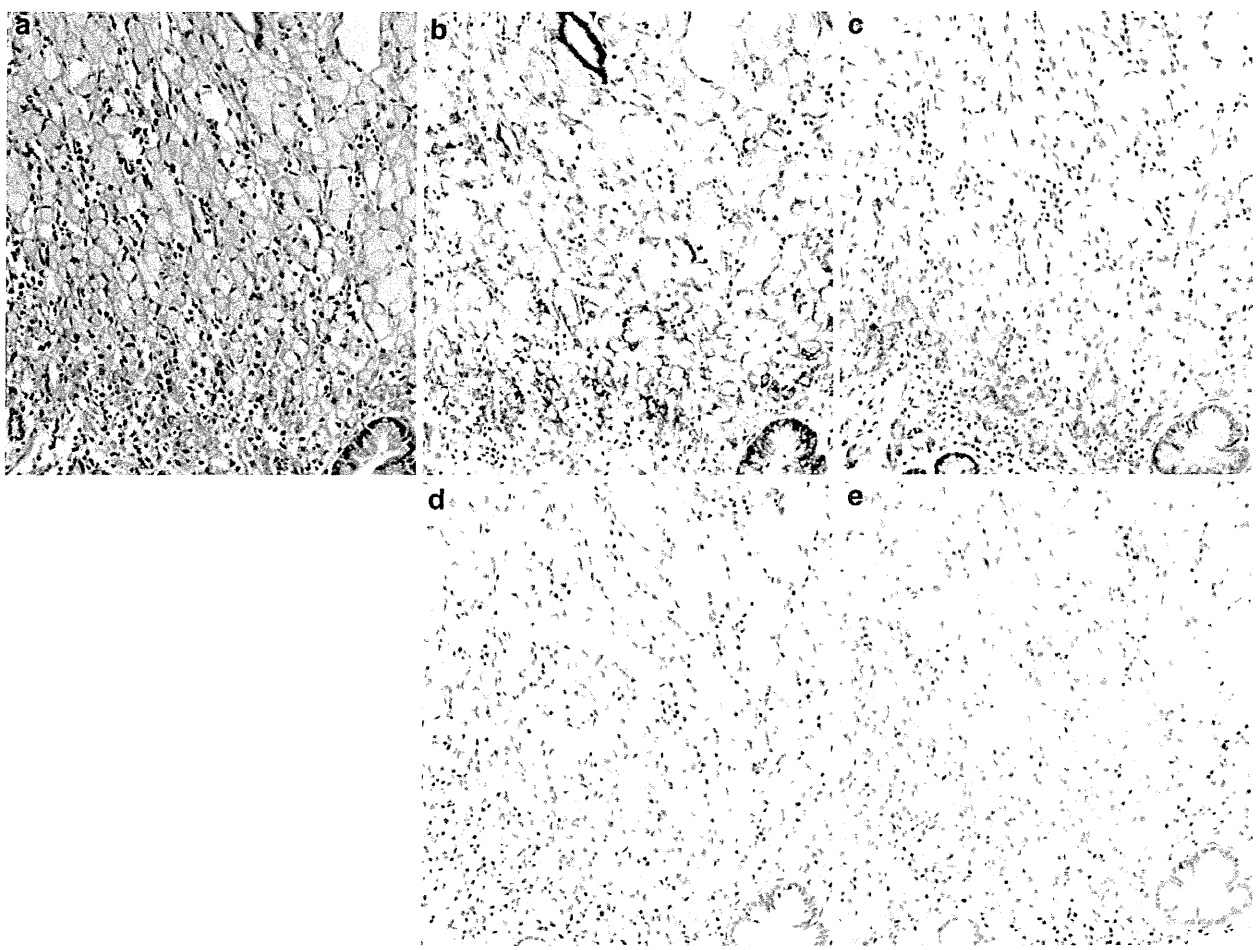

Fig. 1 Pure undifferentiated-type (PURE-type) carcinoma with gastric type (G type). **a** HE staining. MUC5AC (**b**) and MUC6 (**c**) are positive in the cytoplasm. MUC2 (**d**) and CDX2 (**e**) are negative (**a–e**, ×200)

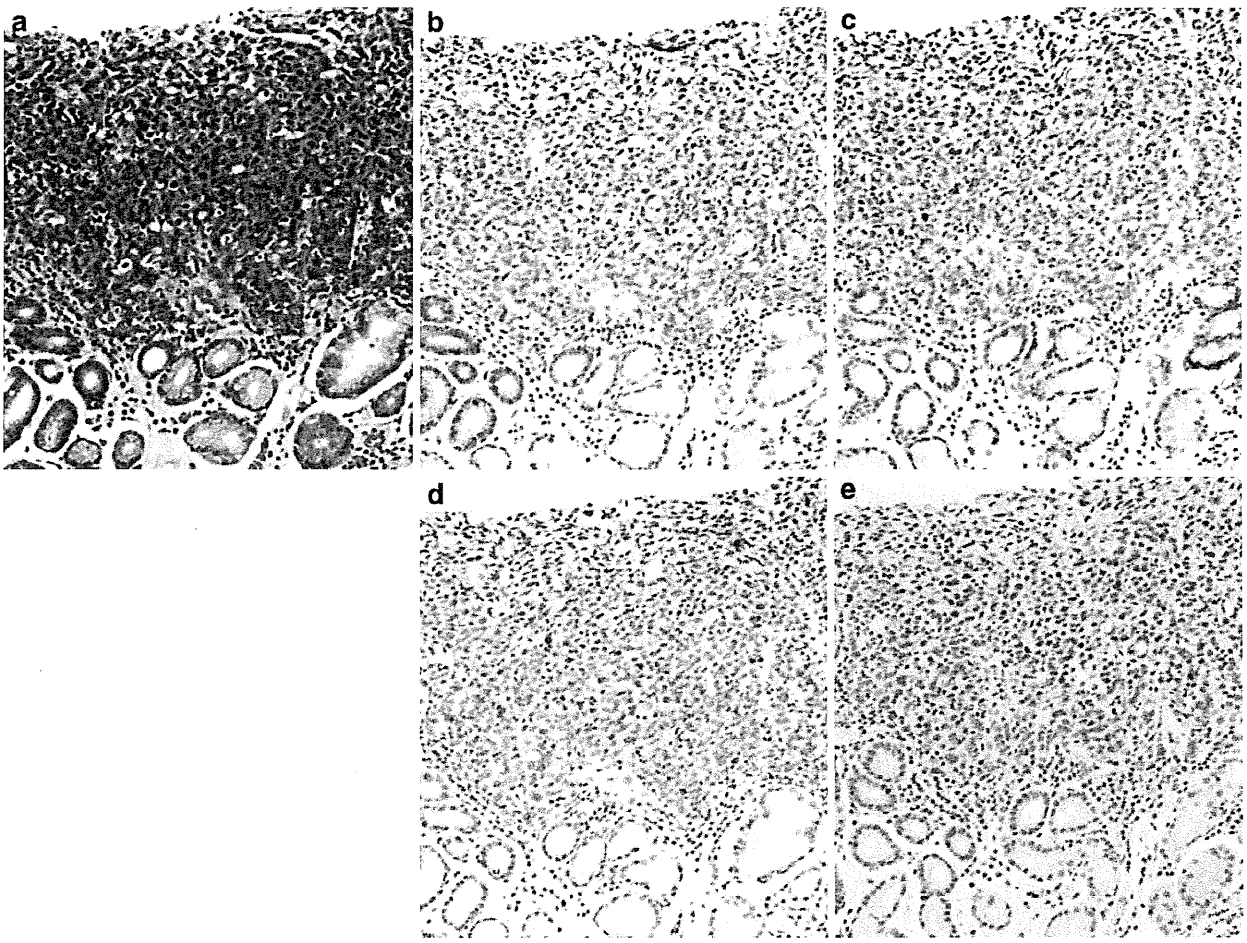

Fig. 2 PURE-type carcinoma with intestinal type (I type). **a** HE staining. MUC5AC (**b**) and MUC6 (**c**) are negative. MUC2 (**d**) is positive in the cytoplasm, and CDX2 (**e**) is positive in the nucleus (**a–e**, ×200)

expression for intestinal markers but negative expression for gastric markers (Fig. 2); (3) gastrointestinal type (GI type), demonstrating positive expression both for gastric and intestinal markers (Fig. 3); and (4) null type (N type), with negative expression for all markers. Furthermore, to compare our findings with previous reports that did not use CDX2 as a phenotypic marker, the carcinoma phenotypes were separately evaluated in two steps: phenotype judged by MUC only, and that judged by MUC and CDX2 combined. In the MIXED-type group, phenotypes in the POR component and in the TUB component were analyzed separately. Similarly, in submucosal invasive tumors, phenotypes of the intramucosal part and of the submucosal part were analyzed separately (Fig. 4).

Evaluation of surrounding mucosa

The surrounding non-neoplastic mucosa within 5 mm of the margins of the carcinoma cells was evaluated with respect to degree of chronic inflammation, polymorphonuclear neutrophil activity, degree of glandular atrophy, and degree of intestinal metaplasia, based on the updated Sydney system [32].

Statistical analysis

Statistical analysis was performed using the χ^2 test, Fisher's exact test, and the unpaired t-test. Bonferroni's method was used for multiple comparisons. All statistical analyses were performed using the PASW statistics 17 software package (SPSS Japan, Tokyo, Japan). A two-tailed p value of less than 0.05 was considered significant.

Results

Clinicopathological findings

The clinicopathological findings of the 106 PURE-type carcinomas and the 104 MIXED-type carcinomas are

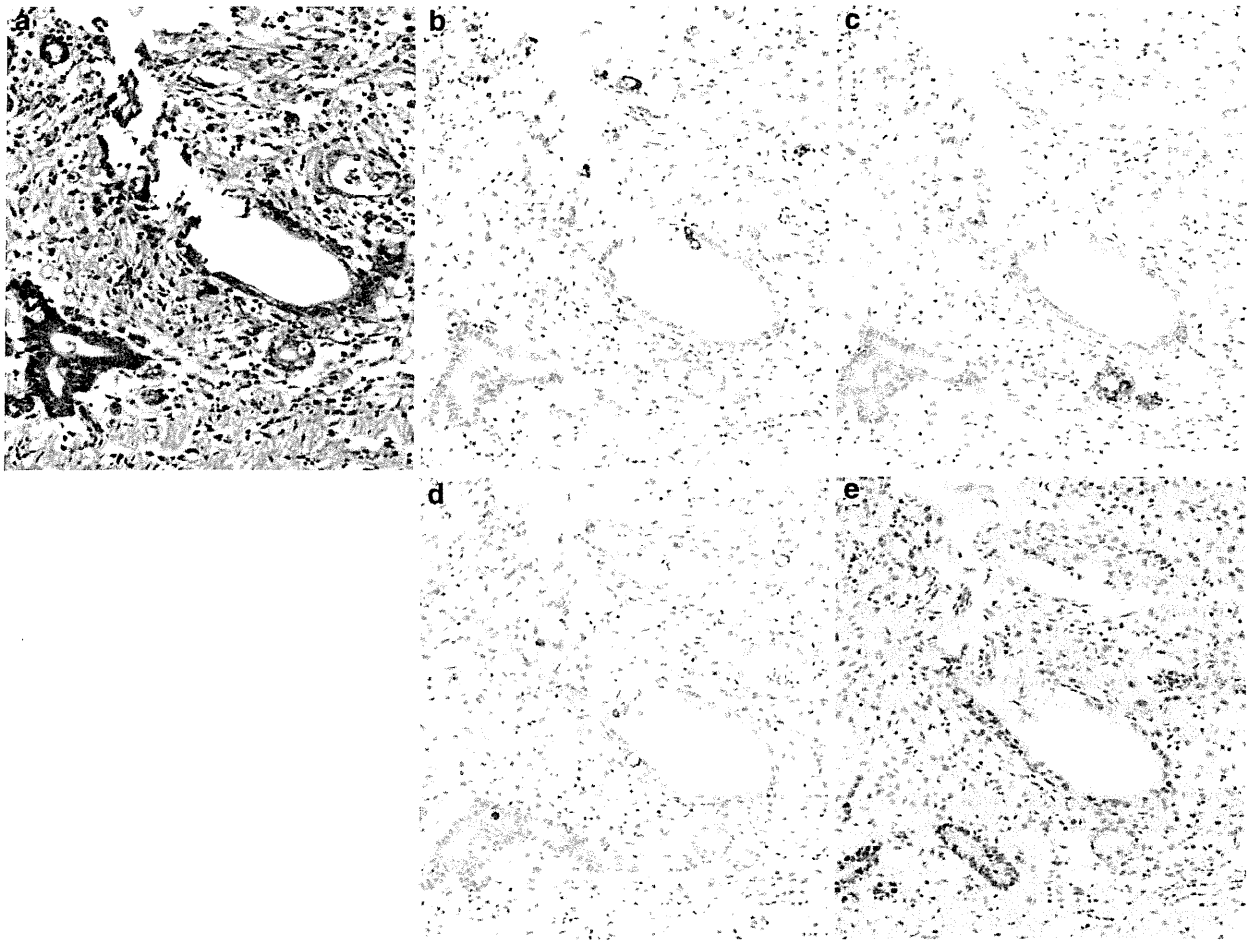

Fig. 3 Mixed differentiated/undifferentiated-type (MIXED-type) carcinoma with gastrointestinal type (GI type). The non-glandular (POR) component is seen in the *right upper side*, and the glandular (TUB) component is seen in the *left lower side* of the lesion. **a** HE staining. In both the POR and TUB components, MUC5AC (**b**), MUC6 (**c**), and MUC2 (**d**) are positive in the cytoplasm, and CDX2 (**e**) is positive in the nucleus (**a**–**e**, ×200)

summarized in Table 1. Submucosal invasive carcinomas were more frequent in the MIXED-type than in the PURE-type ($p < 0.001$). The proportion of male subjects tended to be higher in the MIXED-type than in the PURE-type, but there were no significant differences in age, sex, tumor location, macroscopic type, or tumor size between these two types.

Histopathological findings of surrounding mucosa

The histology of the non-neoplastic surrounding mucosa is summarized in Table 2. The number of PURE-type carcinomas was greater in intermediate-type mucosa than in pyloric gland-type mucosa. Conversely, the number of MIXED-type carcinomas was greater in pyloric gland-type mucosa than in intermediate-type mucosa ($p = 0.017$). MIXED-type carcinomas demonstrated higher intestinal metaplasia scores and significantly higher glandular atrophy scores ($p = 0.035$) than PURE-type carcinomas.

Correlation between histological type and phenotypic expression

The distributions of phenotypes and expressions of phenotypic markers are summarized in Tables 3 and 4. Comparing the two phenotypic classifications (MUC only vs. MUC and CDX2), G type was significantly decreased in the latter (MUC and CDX2) among the three groups (61.3 vs. 17.9 % in PURE-type carcinomas; 59.8 vs. 13.7 % in POR components of MIXED-type carcinomas; 51.0 vs. 11.5 % in TUB components of MIXED-type carcinomas; $p < 0.01$), whereas GI type was significantly increased in the latter (MUC and CDX2) among the three groups (34.9 vs. 78.3 % in the PURE-type carcinomas; 29.4 vs. 75.5 % in the POR components of MIXED-type carcinomas; 44.2

Table 1 Clinicopathological findings of the 210 cases

	PURE-type (n = 106)	MIXED-type (n = 104)	p value
Age, years, mean ± SD (range)	60.1 ± 11.1 (35–86)	60.1 ± 12.5 (26–84)	0.981
Sex (male:female)	51:55	62:42	0.099
Location			0.117
U	16	16	
M	65	49	
L	25	39	
Macroscopic type			0.117
Elevated	8	14	
Flat	16	8	
Depressed	82	82	
Size, mm, mean ± SD (range)	15.7 ± 6.4 (0.4–25.0)	16.7 ± 5.9 (4.0–25.0)	0.226
Depth			<0.001
Intramucosal	76	47	
Submucosal	30	57	

PURE-type pure undifferentiated-type adenocarcinoma, *MIXED-type* Mixed differentiated/undifferentiated-type adenocarcinoma, *U* upper third of the stomach, *M* middle third of the stomach, *L* lower third of the stomach

Table 2 Histopathological findings of the surrounding mucosa of undifferentiated-type adenocarcinomas

	PURE-type (n = 106)	MIXED-type (n = 104)	p value
Type of mucosa			0.017
Fundic-gland type	46	49	
Intermediate-gland type	33	16	
Pyloric-gland type	27	39	
Chronic inflammation (score[a]), mean ± SD	2.45 ± 0.68	2.40 ± 0.63	0.589
Neutrophil activity (score[a]), mean ± SD	1.33 ± 0.88	1.11 ± 0.90	0.070
Atrophy (score[a]), mean ± SD	1.88 ± 0.83	2.12 ± 0.80	0.035
Intestinal metaplasia (score[a]), mean ± SD	1.36 ± 1.11	1.66 ± 1.22	0.059

PURE-type pure undifferentiated-type adenocarcinoma, *MIXED-type* mixed differentiated/undifferentiated-type adenocarcinoma

[a] Updated Sydney system

Table 3 Phenotypic expression of undifferentiated-type adenocarcinomas

	PURE-type (n = 106)	MIXED-type	
		POR (n = 102*)	TUB (n = 104)
Phenotype (MUC only) (%)	[a]	[b]	[c]
G type	65 (61.3)	61 (59.8)	53 (51.0)
GI type	37 (34.9)	30 (29.4)	46 (44.2)
I type	1 (0.9)	3 (2.9)	4 (3.8)
N type	3 (2.8)	8 (7.8)	1 (1.0)
Phenotype (MUC and CDX2) (%)	[d]	[e]	[f]
G type	19 (17.9)	14 (13.7)	12 (11.5)
GI type	83 (78.3)	77 (75.5)	87 (83.7)
I type	2 (1.9)	8 (7.8)	5 (4.8)
N type	2 (1.9)	3 (2.9)	0

PURE-type pure undifferentiated-type adenocarcinoma, *MIXED-type* mixed differentiated/undifferentiated-type adenocarcinoma, *POR* non-glandular component, *TUB* glandular component, *MUC* mucin core protein, *G type* gastric type, *GI type* gastrointestinal type, *I type* intestinal type, *N type* null type

* No intramucosal part in two tumors

[a] vs. [d] and [c] vs. [f], $p < 0.01$ (Fisher's exact test); [b] vs. [e], $p < 0.01$ (χ^2 test)

Table 4 Expression of phenotypic markers in undifferentiated-type adenocarcinomas

	PURE-type (n = 106)	MIXED-type	
		POR (n = 102*)	TUB (n = 104)
Phenotypic marker (%)			
MUC5AC or HGM	100 (96.2)[a]	80 (78.4)[b]	90 (86.5)
MUC6 or M-GGMC-1	73 (70.2)	67 (65.7)	79 (76.0)
MUC2	38 (36.5)	33 (32.4)	50 (48.1)
CDX2	85 (81.7)	85 (83.3)	92 (88.5)

PURE-type pure undifferentiated-type adenocarcinoma, *MIXED-type* mixed differentiated/undifferentiated-type adenocarcinoma, *POR* non-glandular component, *TUB* glandular component, *MUC* mucin core protein

* No intramucosal part in two tumors

[a] vs. [b], $p < 0.01$ (χ^2 test)

vs. 83.7 % in the TUB components of MIXED-type carcinomas; $p < 0.01$). Thus, G type was most common based on MUC only, though GI type was most common based on MUC and CDX2 in each group ($p < 0.01$). However, in both classifications, there was no significant difference in phenotype distribution among the three groups (Table 3).

As for the expression of each phenotypic marker, the positivity rate for MUC5AC was significantly higher in PURE-type carcinomas than in the POR component of MIXED-type carcinomas ($p < 0.01$). The positivity rate for MUC2 tended to be lower in the POR component than in the TUB component of MIXED-type carcinomas. CDX2 expression was detected not only in MUC2-positive cells but also in MUC2-negative cells (Figs. 2, 3), and there were no significant differences in CDX2 expression among the three groups (Table 4).

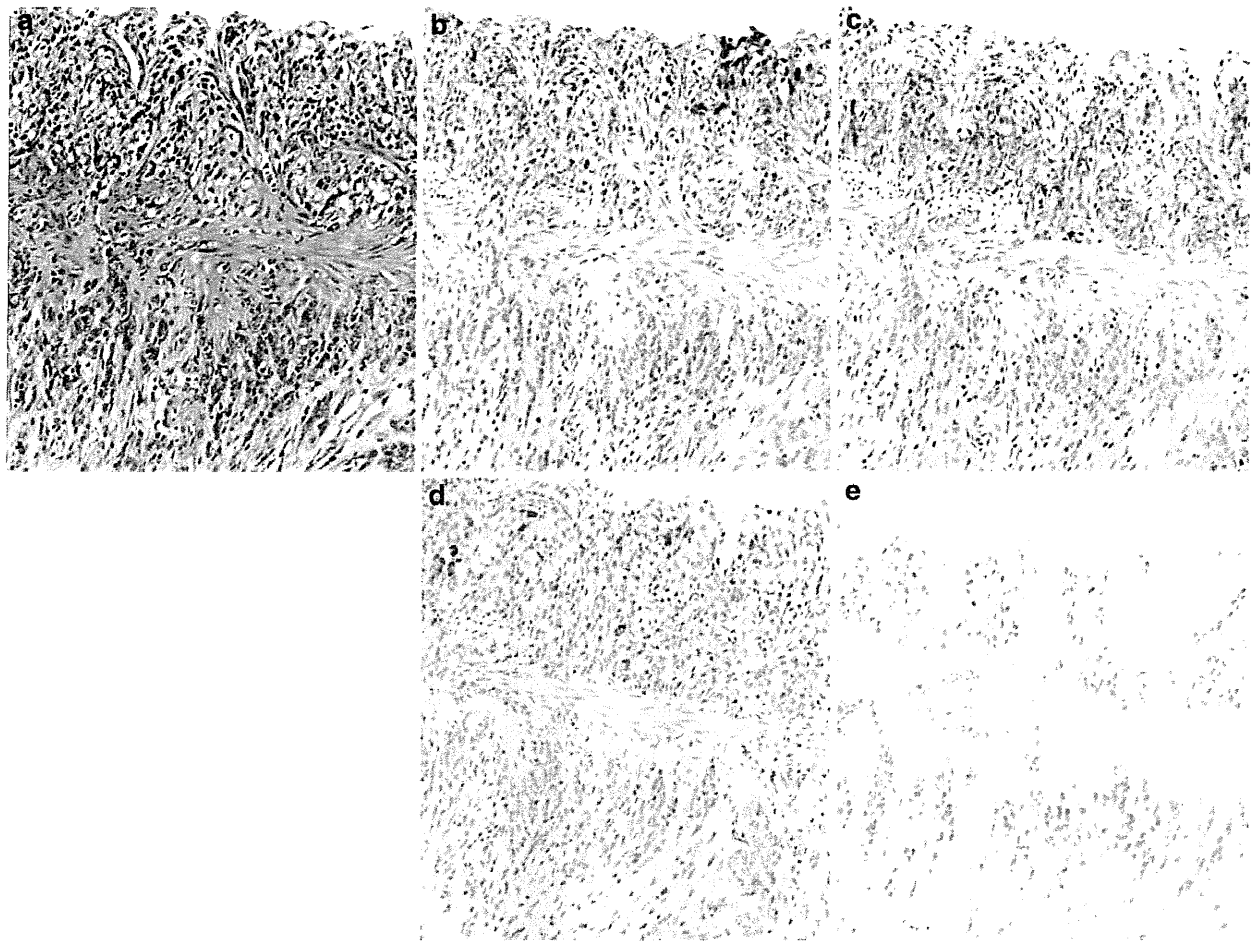

Fig. 4 PURE-type carcinoma with submucosal invasion. The mucosal part is seen in the *upper part*, and the submucosal part is seen in the *lower part* of the lesion. **a** HE staining. MUC5AC (**b**) and MUC6 (**c**) are positive in the mucosal part, but negative in the submucosal part. In contrast, MUC2 (**d**) and CDX2 (**e**) are positive in both the mucosal and submucosal parts (**a**–**e**, ×200)

Correlation between carcinoma size and phenotypic expression

Figure 5 shows the correlation between the phenotypes and the size of carcinomas (≤10 mm and >10 mm) in each of the three groups. In PURE-type carcinomas, G type decreased significantly and GI type increased significantly as carcinoma size increased ($p < 0.05$; Fig. 5a, b). In contrast, both in the POR component and in the TUB component of MIXED-type carcinomas, the prevalence of phenotypes did not change with carcinoma size (Fig. 5d, e, g, h).

In PURE-type carcinomas, the positivity rates for gastric markers were generally stable, whereas the positivity rates for intestinal markers increased as carcinoma size increased; the positivity rate for CDX2 was significantly higher in the >10-mm group than in the ≤10-mm group ($p < 0.05$), and MUC2 expression showed similar changes (Fig. 5c). In contrast, in the POR and TUB components of MIXED-type carcinomas, the positivity rates for gastric and intestinal markers were generally stable regardless of carcinoma size; there was no significant difference in the positivity rate for each phenotypic marker by tumor size (Fig. 5f, i).

Correlation between depth of carcinoma invasion and phenotypic expression

Figure 6 shows the phenotype relationship between the intramucosal and submucosal parts in submucosal carcinoma. In PURE-type carcinomas, the GI type decreased and both the G type and I type increased during carcinoma invasion from the intramucosal to submucosal parts, and the difference was significant when the phenotype was judged by MUC and CDX2 ($p < 0.05$). In the TUB component of MIXED-type carcinomas, there was also a decrease of GI type and an increase of G type and I type during submucosal carcinoma invasion, and the differences

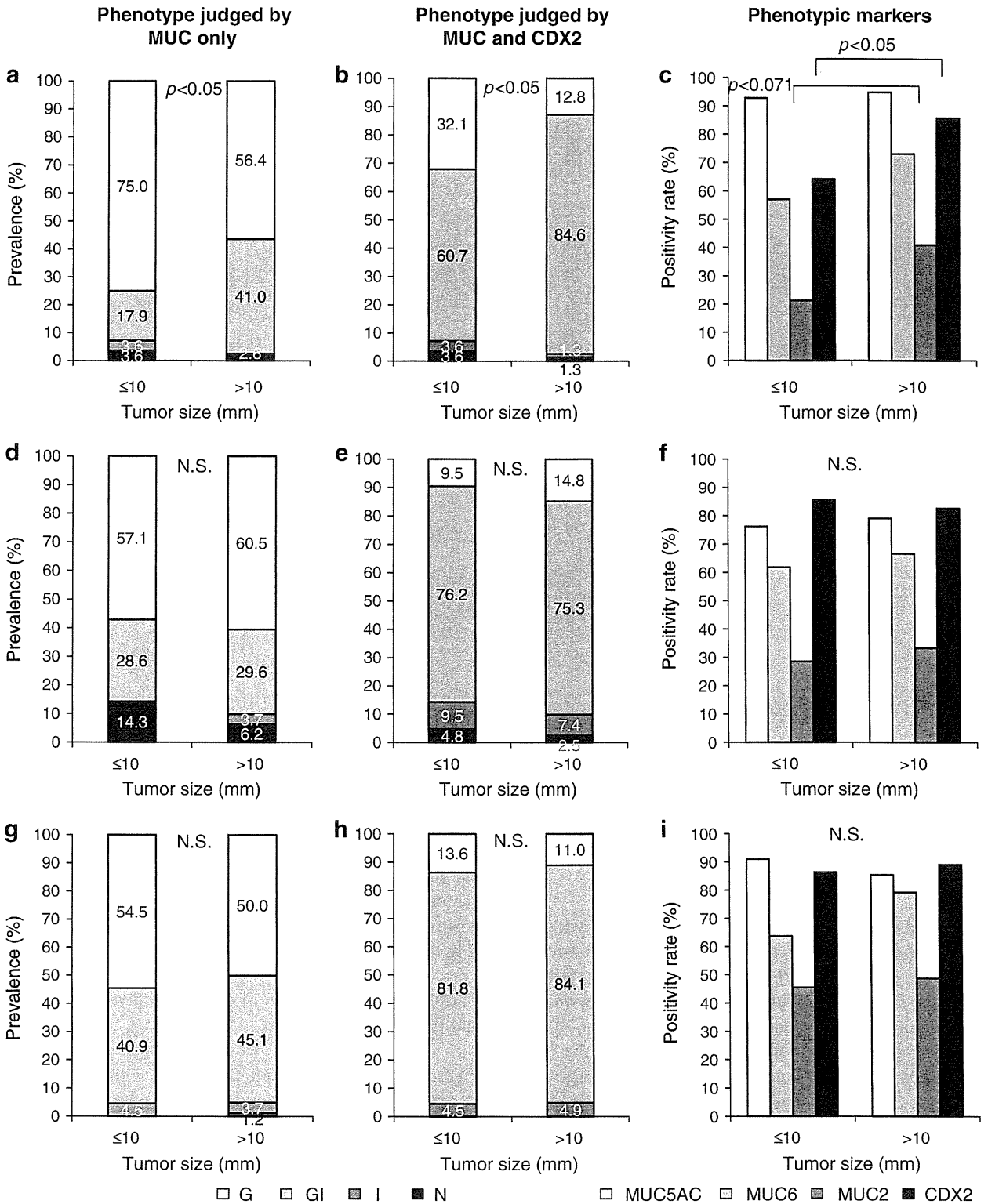

Fig. 5 Differences in phenotypic expression by carcinoma size. Phenotype prevalence using mucin core protein (MUC) only and using MUC and CDX2 combined, and the positivity rate for phenotypic markers in the PURE-type (**a–c**), the POR component of the MIXED-type (**d–f**), and the TUB component of the MIXED-type (**g–i**). *N.S.* not significant

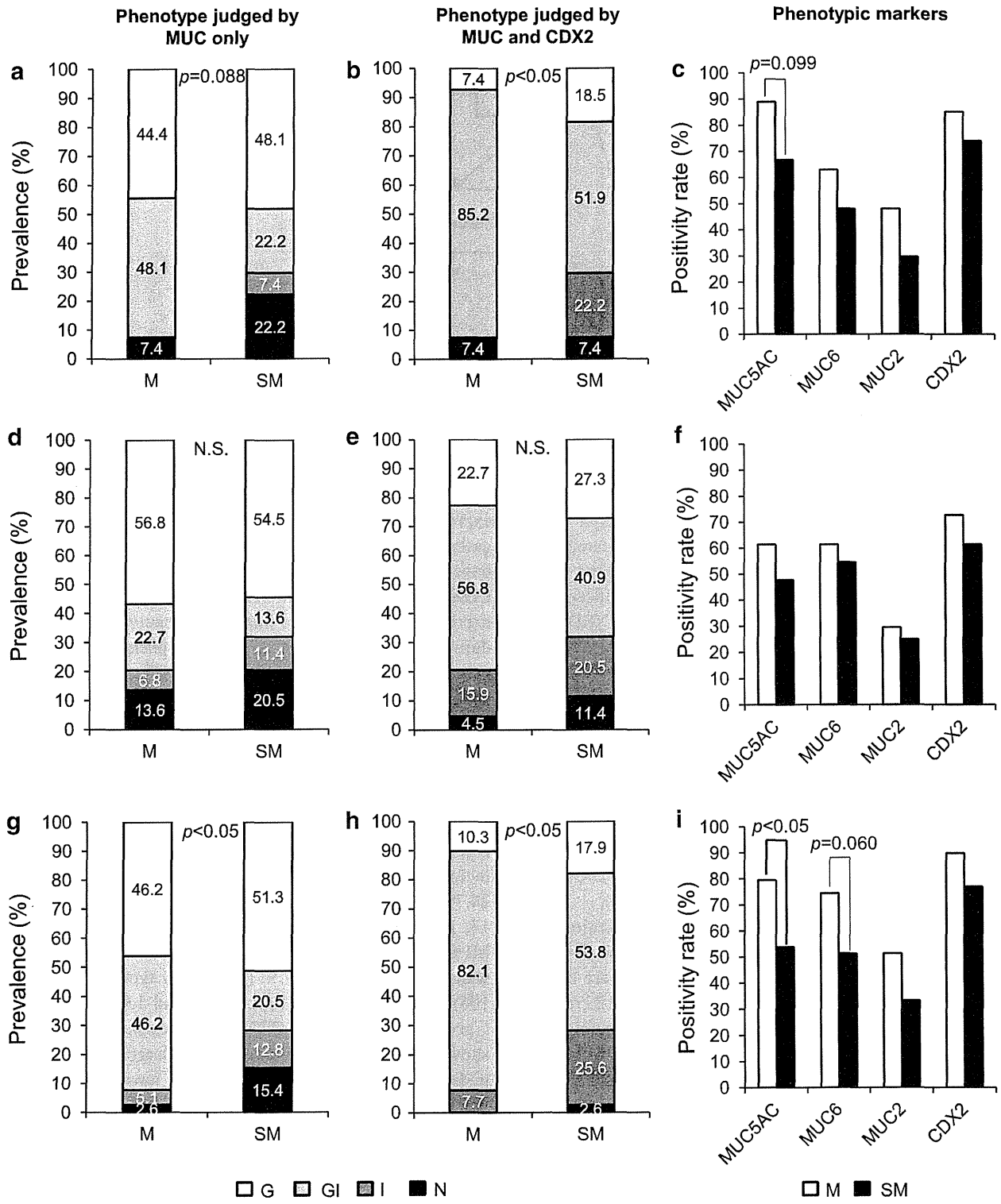

Fig. 6 Differences in phenotypic expression according to depth of carcinoma invasion. *M* intramucosal part, *SM* submucosal part. Phenotype prevalence using MUC only and using MUC and CDX2 combined, and positivity rates for phenotypic markers in PURE-type (**a–c**), the POR component of the MIXED-type (**d–f**), and the TUB component of the MIXED-type (**g–i**)

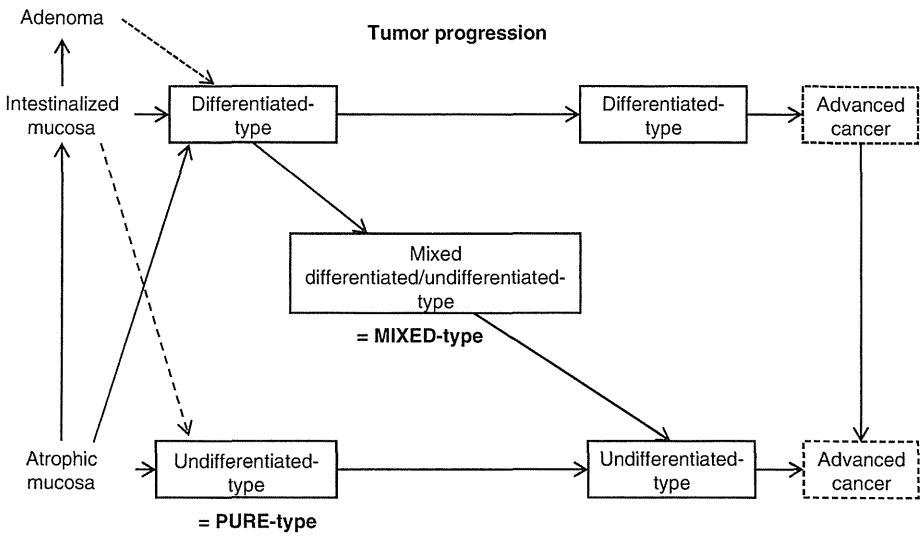

Fig. 7 Schema of assumed pathways in tumorigenesis and development of gastric adenocarcinomas

were significant regardless of the use of CDX2 ($p < 0.05$; Fig. 6a, b, g, h).

The positivity rate for each phenotypic marker, especially gastric markers, tended to decrease during carcinoma invasion from the intramucosal to submucosal parts in all three groups (Fig. 4); this tendency was significant for MUC5AC in the TUB component of MIXED-type ($p < 0.05$; Fig. 6c, f, i).

Discussion

A total of 210 lesions of undifferentiated-type early gastric adenocarcinoma less than 25 mm in diameter were immunohistochemically investigated based on mucin core proteins and CDX2 to clarify the differences between two groups of different development pathways (PURE-type carcinoma and MIXED-type carcinoma) (Fig. 7).

As previously reported [8, 29–31], the distribution and positivity of MUC5AC and HGM, as well as the distribution and positivity of MUC6 and M-GGMC-1, are different. In brief, of the foveolar-type mucins, MUC5AC is detected more often than HGM mucin in gastric carcinoma, because MUC5AC is basically limited to being within the cytoplasm, while HGM is confined to the luminal surface coat, as well as the cytoplasm, of gastric carcinomas. Of the pyloric gland-type mucins, MUC6 mucin is more abundant than M-GGMC-1 mucin and is restricted to the cytoplasm, whereas M-GGMC-1 mucin is sometimes found on the luminal surface coat, as well as in the cytoplasm. Therefore, in the present study, MUC5AC, HGM, MUC6, and M-GGMC-1 stains were all used to accurately determine the mucin phenotypes of gastric carcinomas. Furthermore, CDX2 was used as an intestinal phenotype marker along with MUC2. The positivity rate was higher for CDX2 than for MUC2, and CDX2 expression was detected in cancerous areas not only where MUC2 expression was apparent, but also in tissues exhibiting only gastric markers or null phenotypic lesions. Previous reports have shown that there is a positive correlation between CDX2 expression and MUC2 [21, 33], and that CDX2 expression might precede intestinal phenotypic expression during a shift from gastric to intestinal phenotype with the progression of gastric carcinomas [17]. Thus, CDX2 appears to be a more sensitive marker than MUC2 for assessing the presence of intestinal phenotypic expression.

Based on MUC only, PURE-type carcinomas were classified as 61.3 % (65/106) G type, 34.9 % (37/106) GI type, 0.9 % (1/106) I type, and 2.8 % (3/106) N type. Previous reports have shown the rates of the G, GI, I, and N types of early undifferentiated-type adenocarcinoma, including signet-ring cell carcinoma, to be 27.8–62.4 %, 24.7–68.5 %, 0–23.1 %, and 0–10.8 %, respectively [9, 10, 13, 14, 17, 26]. In contrast to the above findings based on MUC only, PURE-type carcinomas in the present study were classified into 17.9 % (19/106) G type, 78.3 % (83/106) GI type, 1.9 % (2/106) I type, and 1.9 % (2/106) N type based on MUC and CDX2. The present results clearly showed that there was an unexpectedly larger population of undifferentiated-type adenocarcinomas having the intestinal phenotype or gastrointestinal phenotype as compared with previously reported phenotypes based on MUC without the use of CDX2.

On the other hand, there are some reports [17–19, 33] suggesting a possible tumor suppressor role for CDX2, but the significance of CDX2 expression in gastric neoplasms is still under debate. The present study targeted the expression of mucin phenotype, and the materials used were limited to early-stage gastric carcinomas sized 25 mm or less, which made it difficult to evaluate biological

behavior or patient prognosis. Further studies with larger numbers of lesions, including advanced-stage lesions, are required to clarify the relationship between phenotype expression and biological significance.

We found that PURE-type carcinomas more frequently arose in fundic glands and intermediate-type mucosa than in pyloric gland-type mucosa. The background mucosa of the MIXED-type carcinoma demonstrated a higher intestinal metaplasia score and a significantly higher glandular atrophy score than that of PURE-type carcinoma. These findings seem to suggest that PURE-type carcinoma arises from ordinary gastric mucosa with mild glandular atrophy and intestinal metaplasia, while MIXED-type carcinoma arises from intestinalized mucosa with much glandular atrophy, regardless of phenotypic expression.

PURE-type carcinomas showed the gastric phenotype in 32.1 % of cases when their size was $\leq$10 mm, considered to be a very early stage of carcinogenesis. Furthermore, they also demonstrated a size-dependent increase in intestinal phenotypic markers (CDX2 and MUC2) but no correlation for gastric phenotypic markers, resulting in increased GI phenotype as tumor size increased (Fig. 5). In contrast, in MIXED-type carcinomas, the intramucosal part showed intestinal phenotypic expression even in smaller-sized carcinomas (Fig. 5). These results may allow us to consider that not a small number of PURE-type carcinomas arise with pure gastric phenotype and acquire the intestinal phenotype during mucosal development; on the other hand, a large number of MIXED-type carcinomas have the intestinal phenotype from the very early stage of carcinogenesis, and intestinal phenotypic expression tends to be reduced with morphological alteration (Fig. 7). Bamba et al. [14] reported time- (size-) dependent expression of the intestinal phenotype in signet-ring cell carcinomas. Natsagdorj et al. [22] reported that the undifferentiated-type gastric carcinomas derived from signet-ring cell carcinomas and the undifferentiated-type gastric carcinomas derived from differentiated-type carcinomas showed differences in intestinal phenotypic marker expressions.

In the present study, the proportion of GI type decreased and that of G and I type increased as carcinoma developed from the intramucosal to submucosal parts, and phenotypic marker expression, especially gastric markers, tended to decrease (Fig. 6). Each case, except for one (data not shown), individually showed phenotypic alteration with reduction of gastric and intestinal markers during submucosal invasion. These findings may suggest that the increased proportion of I type during submucosal invasion is caused not by the acquisition of intestinal marker expression, but by a reduction of gastric marker expression. In contrast, previous reports have shown that the phenotype of signet-ring cell carcinomas alters from gastric phenotype to intestinal phenotype during submucosal invasion [11–13]. It may be argued that reduced gastric phenotypic expression in the submucosal part could be caused by the selective submucosal invasion of constitutively non-gastric-type cells. However, this seems unlikely, because the pattern of phenotypic expression in tumor cells right under the muscularis mucosae was the same as that in the intramucosal part, and the submucosal part showed gradual loss of phenotypic expression. Similarly, Nakamura et al. [34] reported the loss of gastric and intestinal phenotypic expression during tumor progression in differentiated-type early gastric carcinomas. Natsagdorj et al. [22] reported that intestinal phenotypic expression was reduced with deeper extramucosal invasion, due to loss of induction by the tissue environment, in undifferentiated-type gastric carcinomas.

In conclusion, CDX2 was a more sensitive marker than MUC2 for assessing the presence of intestinal phenotypic expression from the early stage in undifferentiated-type gastric adenocarcinomas. The present data suggest that there are two different groups of undifferentiated-type gastric adenocarcinomas, PURE-type carcinomas and MIXED-type carcinomas, according to phenotype expression. It is possible that these two groups develop via different tumorigenesis pathways with differences in phenotypic alteration during tumor progression.

Acknowledgments The authors would like to thank all the members of our laboratory for their technical assistance, especially Miss Kazue Kobayashi for her excellent immunohistochemical work.

Conflict of interest The authors have no conflicts of interest to disclose.

References

1. Lauren P. The two histological main types of gastric carcinoma: diffuse and so-called intestinal-type carcinoma. An attempt at a histo-clinical classification. Acta Pathol Microbiol Scand. 1965;64:31–49.
2. Nakamura K, Sugano H, Takagi K. Carcinoma of the stomach in incipient phase: its histogenesis and histological appearances. Gann. 1968;59(3):251–8.
3. Correa P. A human model of gastric carcinogenesis. Cancer Res. 1988;48(13):3554–60.
4. Correa P. Human gastric carcinogenesis: a multistep and multifactorial process—First American Cancer Society Award Lecture on Cancer Epidemiology and Prevention. Cancer Res. 1992;52(24):6735–40.
5. Tatematsu M, Ichinose M, Miki K, Hasegawa R, Kato T, Ito N. Gastric and intestinal phenotypic expression of human stomach cancers as revealed by pepsinogen immunohistochemistry and mucin histochemistry. Acta Pathol Jpn. 1990;40(7):494–504.
6. Kushima R, Hattori T. Histogenesis and characteristics of gastric-type adenocarcinomas in the stomach. J Cancer Res Clin Oncol. 1993;120(1–2):103–11.
7. Kabashima A, Yao T, Sugimachi K, Tsuneyoshi M. Gastric or intestinal phenotypic expression in the carcinomas and background mucosa of multiple early gastric carcinomas. Histopathology. 2000;37(6):513–22.